



Coupled longitudinal/lateral controllers for autonomous vehicles navigation, with experimental validation

Alia Chebly, Reine Talj, Ali Charara

► To cite this version:

Alia Chebly, Reine Talj, Ali Charara. Coupled longitudinal/lateral controllers for autonomous vehicles navigation, with experimental validation. *Control Engineering Practice*, 2019, 88, pp.79-96. 10.1016/j.conengprac.2019.05.001 . hal-02407330

HAL Id: hal-02407330

<https://hal.science/hal-02407330>

Submitted on 6 Jan 2021

HAL is a multi-disciplinary open access archive for the deposit and dissemination of scientific research documents, whether they are published or not. The documents may come from teaching and research institutions in France or abroad, or from public or private research centers.

L'archive ouverte pluridisciplinaire **HAL**, est destinée au dépôt et à la diffusion de documents scientifiques de niveau recherche, publiés ou non, émanant des établissements d'enseignement et de recherche français ou étrangers, des laboratoires publics ou privés.

Coupled longitudinal/lateral controllers for autonomous vehicles navigation, with experimental validation

Alia Chebly, Reine Talj, Ali Charara

Abstract—In this work, the coupled control of the lateral and the longitudinal dynamics of an autonomous vehicle is addressed. As a first step, a multi-body modeling technique is used to develop a four wheeled vehicle planar model. This technique considers the vehicle as a robot consisting of articulated bodies. The geometric description of the vehicle system is derived using the modified Denavit Hartenberg parameterization and then the dynamic model of the vehicle is computed by applying a recursive method used in robotics, namely Euler-Lagrange based Algorithm. The validation of the developed vehicle model was then conducted using an automotive simulator, the Scaner-Studio simulator.

The developed vehicle model is then used to derive coupled control laws for the lateral and the longitudinal vehicle dynamics. Two coupled controllers are proposed: In the first controller, the control is realized using Lyapunov control techniques while in the second one an Immersion and Invariance with sliding mode approach is used. Both of the controllers aim to ensure a robust tracking of the reference trajectory and the desired speed while taking into account the strong coupling between the lateral and the longitudinal vehicle dynamics. In fact, the coupled controller is a key step for the vehicle safety handling, especially in coupled maneuvers such as lane-change maneuvers, obstacle avoidance maneuvers and combined maneuvers in critical driving situations.

The developed controllers were validated in simulation under Matlab/Simulink using experimental data. Subsequently, an experimental validation of the proposed controllers was conducted using a robotized vehicle (Renault-ZOE) present in the Heudiasyc laboratory within the Equipex Robotex project.

Index Terms—Autonomous vehicles, coupled control, robotics modeling, reference tracking, speed tracking.

I. INTRODUCTION

THE development of autonomous vehicles has received a lot of attention during the last decades, not only in the research field, but also in the industry, academic and military fields. The motivation is to guarantee a reliable and secure vehicle navigation even in critical driving situations. Indeed, the vehicle autonomy can be accomplished by three main steps: The perception and localization, the trajectory planning and the vehicle control.

This work treats the vehicle control module and aims to propose new solutions that can enhance the safety of an autonomous vehicle. Indeed, several control techniques can be found in the literature but most of these techniques address the

A. Chebly, R. Talj and A. Charara are with Sorbonne universités, Université de technologie de Compiègne, CNRS, Heudiasyc UMR 7253, CS 60 319, 60 203 Compiègne, France. e-mails: alia.chebly@hds.utc.fr, reine.talj@hds.utc.fr, ali.charara@hds.utc.fr

lateral control ([1], [2], [3], [4], [5], [6]) and the longitudinal control ([7], [8], [9], [10], [11], [12]) of the vehicle dynamics separately.

Actually, the vehicle dynamics are strongly coupled, and in order to control the vehicle and handle its safety and stability, these dynamics coupling should be taken into account when designing the vehicle controller. Recently, some research groups are addressing the problem of controlling the lateral and the longitudinal vehicle dynamics in a coupled way. In [13], a coupled longitudinal and lateral control based on a sliding mode technique is proposed. The idea is to calculate the desired tire forces to obtain the steering angle by inverting the tire model. Note that the analytical inversion of the tire model is not possible, which makes the operation somehow complex. Beside this, their solution requires an estimation of the slip ratio and since this estimate is unavailable, only the proposed lateral controller is experimentally tested. Recently, a solution based on the flatness control theory has been proposed in [14]. The proposed controller is validated by simulations using noisy experimental data, which were acquired by a laboratory vehicle with highly dynamic loads and high lateral accelerations. Another solution based on a backstepping synthesis is proposed in [4]. The proposed controller validation is conducted by a simulation using data from a real experimentation. In [15], a global guidance strategy is proposed. The lateral guidance is accomplished using a Nonlinear Model Predictive Control strategy. The proposed solution is validated through simulations showing promising results.

Indeed, the challenge is to design coupled controllers that are at the same time simple, allowing their implementation on a real vehicle and their execution in real-time, and robust, by taking into account the strong coupling between the lateral and the longitudinal vehicle dynamics.

In this work, this problem is also addressed and two new solutions are proposed: The first coupled controller is developed based on Lyapunov control techniques while the second coupled controller is based on Immersion and Invariance with sliding mode control technique.

These new solutions were validated by simulation under Matlab/Simulink and experimentally on a robotized vehicle within the Heudiasyc laboratory.

The controllers design makes use of a four wheeled vehicle model that is developed using a multi-body formalism based on Euler-Lagrange algorithm. Indeed, several methods were

proposed in the literature to model the vehicle kinematics and dynamics. The well-known models are the kinematic bicycle model [16], [17], the dynamic bicycle model [18] and the four wheels model [19]. These closed-form models are developed using the fundamental principles of physics such as Newton-laws and most of them are built on simplifying kinematic constraints or neglecting some dynamic aspects.

Lately, some advanced models have been developed using multi-body systems to model a complex system. The main advantage of the multi-body modeling technique is its accuracy with respect to the simplified closed-form models. Multi-body models usually provide more information, which are usually neglected when using a closed-form model.

In [20], R.S. Sharp provided a model for a two wheeled vehicle (motorcycles) with the aim of developing new control tools to improve the motorcycles stability. Also, Cossalter et al [21] developed a model based on the Lagrange Formalism that consists of interconnected rigid bodies together with suspensions and sophisticated tire and engine models. In [22], E. Sanjurjo uses an index-3 augmented Lagrangian formulation with mass-orthogonal projections [23], [24] to model the vehicle. Lately, in [25], S. Maakaroun used a recursive formulation, namely the Euler-Lagrange method, to model the vehicle. They proceed in a systematic geometrical description in order to obtain the vehicle model directly with a minimum number of numerical steps. This recursive method was used to develop a two-wheeled and a four-wheeled vehicle models in [26], and then a narrow tilted vehicle model in [26]. In [27], this same formalism was used to identify the vehicle parameters. G. Max [28] also used a recursive formulation to model the vehicle, namely the Appell's method based on the Gibbs function (acceleration energy).

Actually, the recursive formalism used in [25] assimilates the vehicle to a robot with multiple bodies related by joints and interacting between them. This modeling technique leads to a more accurate and complete model than the classical modeling tools and that's why it was chosen in this work.

Among the mutli-body modeling technique, we have chosen to proceed with the recursive formulation developed in [25] and based on the method of Luh, Walker and Paul [29], where Euler-Lagrange dynamics are used to derive the dynamic model of the vehicle. This formulation was adopted since it allows to automatically calculate the symbolic expressions of the dynamic model with a minimum number of numerical steps. Moreover, the algorithm complexity does not increase with the system's complexity (large number of variables) and the modification of the system's assumptions can be taken into account in a simple way (For example, the consideration or not of some components of the system).

This paper is organized as follows: Section II presents the vehicle modeling technique and the validation of the developed model. In section III, we present the developed coupled controllers while we present in section IV the controllers validations by simulation and by experimentation. Finally, Section V concludes the paper.

II. VEHICLE MODELING

A. Methodology

The system is modeled using the multi-body formalism used in [25], [30]. This formalism considers the vehicle as a multi-articulated system consisting of n bodies wherein the chassis is the movable base and the wheels are the terminals. Each body is connected to its antecedent by a joint which represents a translational or a rotational degree of freedom. Some virtual bodies are introduced to describe the joints with multiple degrees of freedom or to introduce intermediate fixed frames (see Fig. 1,2).

The geometrical description of the vehicle is based on the modified Denavit-Hartenberg (DHM) notation. The vehicle dynamic model is then computed using a mixed Euler-Lagrange formalism. This formalism is named so, since the chassis variables are represented using Euler variables (COG positions: X,Y and Z, and Euler angles: roll, pitch and yaw), while the other articulations are represented using Lagrangian variables.

The dynamic model is then obtained using the method of Luh, Walker and Paul [29]. This method consists of two recurrences, where the Newton-Euler equations are computed as follows: The forward recursive equations, from the mobile base to the effectors, compute the total forces and moments (jF_j and jMo_j) on each link (j) by calculating the angular and the linear speeds and accelerations of each body (C_j); The backward recurrence, from the effectors to the mobile base, computes the forces and the moments (jf_j and jmo_j) applied on each body by its antecedent taking into account the external forces applied to the robot.

In order to compute the torque τ_j applied on the body C_j , we project the vector of forces jf_j or moments jmo_j (according to the type of the joint j) on the axle of movement.

$$\tau_j = (\sigma_j {}^jf_j + \bar{\sigma}_j {}^jmo_j)^{tj} a_j \quad (1)$$

where ${}^ja_j = [0 \ 0 \ 1]^t$, $\sigma_j = 1$ if the joint j is translational, $\sigma_j = 0$ if the joint j is rotational and $\sigma_j = 2$ if the frame is fixed to a virtual body. The reader can refer to [25] and [30] for more details.

The computation of the vector of the actuators torques τ permits to express the inverse dynamic model of the vehicle as follows:

$$\tau = f(q, \dot{q}, \ddot{q}, f_e) = A(q)\ddot{q} + H(q, \dot{q}) + J(q)f_e \quad (2)$$

where q , \dot{q} and \ddot{q} are the vectors of positions, speeds and accelerations of all the joints including the variables of the chassis. J is the jacobian matrix and Jf_e is the vector of generalized efforts representing the projection of external forces (f_e) on the joint axis. H is the vector of centrifugal, coriolis and gravity terms, and A is the system's inertial matrix.

The direct dynamic model is then derived by calculating the matrices A , H and J from (2) as follows:

- The column c_a of the matrix A is computed by

$$A(:, c_a) = \frac{\partial \tau}{\partial \ddot{q}(c_a)}, \quad c_a \in [1, l], \quad (3)$$

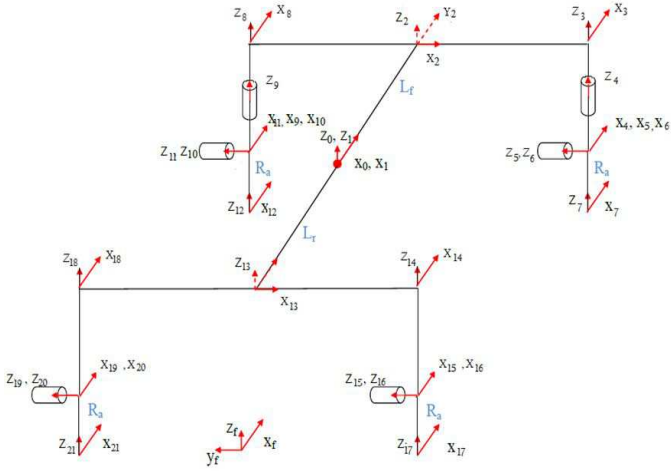


Fig. 1: Poly-articulated system with 21 bodies and 7 degrees of freedom.

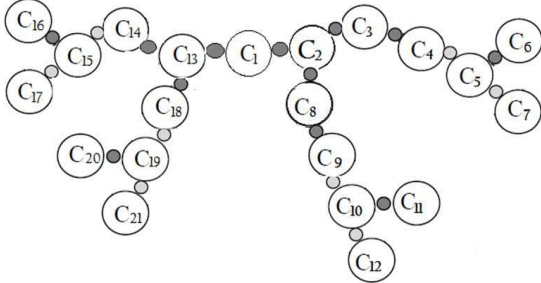


Fig. 2: Model topology with 21 bodies.

where l represents the number of degrees of freedom in the system which is the dimension of the vector q .

- The matrix J is computed similarly by

$$J(:, c_j) = \frac{\partial \tau}{\partial f_e(c_j)}, \quad c_j \in [1, r_f], \quad (4)$$

where r_f represents the dimension of the vector f_e .

- The matrix H is obtained using $H(q, \dot{q}) = \tau$ when $\ddot{q} = f_e = 0$. Then,

$$H = f(q, \dot{q}, 0, 0) \quad (5)$$

B. Four Wheels Vehicle Model

Some assumptions were made compared to a standard automobile model. These assumptions are listed below:

- The track and the wheelbase do not vary;
- The linkage efforts of the front and the rear axles of the vehicle are not taken into account;
- The steering is due to the rotation of the steering wheel and the dynamics of the steering column is not taken into account.
- The pneumatic torsor is applied at the surface of contact between the tire and the ground.
- The road is considered a horizontal plane.

The kinematic chain of the vehicle system has a tree structure. Its base is the vehicle chassis and its terminals are the vehicle

wheels. In fact, the added virtual bodies (C_7, C_{12}, C_{17} and C_{21}), which role is explained below, are also considered as terminals for the vehicle system. It results that the vehicle is modeled by a robot of a tree structure with one basis and eight terminals (four wheels and four virtual bodies) (Fig. 2).

Indeed, the developed model is composed of 21 bodies (Fig. 1,2) defined as follows:

- C_1 represents the vehicle's chassis
- $C_2, C_3, C_8, C_{13}, C_{14}$ and C_{18} are virtual bodies introduced as intermediate fixed frames
- C_4 and C_9 are the front right and the front left steering columns respectively
- $C_5, C_{10}, C_{15}, C_{19}$ are virtual bodies fixed to the four wheels by blocked joints
- C_6, C_{11}, C_{16} and C_{20} are the front right, front left, rear right and rear left wheels respectively
- C_7, C_{12}, C_{17} and C_{21} are virtual bodies fixed to the four wheels.

To explain the role of the virtual bodies related to the wheels, let's take for example the bodies related to the front right wheel (C_5, C_6 and C_7). The virtual bodies C_5 and C_7 are introduced to indicate that the wheels are in rotation around their axes while maintaining their contact with the ground. The contact forces between the wheel and the ground are computed in the frame of the virtual body C_7 , which is linked to the fixed virtual body C_5 . This means that the frame representing the contact Tire/road is not rotating with the wheel. The body C_6 is related to the wheel and represents the wheel rotation in its frame. The wheel equations of motion are then taken on the fixed virtual body C_5 in order to take into account the wheel rotation and the forces generated in the contact zone between the wheel and the ground. The same reasoning is applied to the four wheels.

Seven degrees of freedom are considered, $q = [x \ y \ \psi \ \theta_{fl} \ \theta_{fr} \ \theta_{rl} \ \theta_{rr}]^t$, where x and y are the longitudinal and the lateral positions of the vehicle computed in the vehicle frame R_0 , at the vehicle's center of gravity (COG). ψ is the vehicle's yaw angle, θ_{ij} is the angular position of the wheel ij , where ij stands for front right (fr), front left (fl), rear right (rr) and rear left (rl).

The most significant external forces applied to the vehicle model are the contact forces between the ground and the tires. These forces are modeled using Dugoff's model ([31]) since this model can be considered as a good compromise in terms of simplicity and representativity. It takes into account the coupling between the lateral and the longitudinal forces, the friction coefficient, the wheels adhesion and stiffness, the slip ratio and the vertical forces. We also take into consideration the longitudinal aerodynamic force (F_{aero}) since its effect can't be neglected for high vehicle speeds. This force is given by:

$$F_{aero} = 1/2 \rho_a c_d s \dot{x}^2 \quad (6)$$

where ρ_a is the mass density of air, s is the frontal area of the vehicle, c_d is the aerodynamic drag coefficient and \dot{x} is the longitudinal vehicle speed.

The developed dynamic model is then given by:

$$\ddot{q} = [A(q)]^{-1}(\tau - H(q, \dot{q}) - J(q)f_e). \quad (7)$$

where the matrices A, H and J are as follows:

$$A = \begin{pmatrix} m & 0 & 0 & 0 & 0 & 0 & 0 \\ 0 & m & -L_3 & 0 & 0 & 0 & 0 \\ 0 & -L_3 & I_3 & 0 & 0 & 0 & 0 \\ 0 & 0 & 0 & I_w & 0 & 0 & 0 \\ 0 & 0 & 0 & 0 & I_w & 0 & 0 \\ 0 & 0 & 0 & 0 & 0 & I_w & 0 \\ 0 & 0 & 0 & 0 & 0 & 0 & I_w \end{pmatrix}, \quad (8)$$

$$H = \begin{pmatrix} -m\dot{\psi}\dot{y} + L_3\dot{\psi}^2 \\ m\dot{\psi}\dot{x} \\ -L_3\dot{\psi}\dot{x} \\ 0 \\ 0 \\ 0 \\ 0 \end{pmatrix}, \quad (9)$$

and $J = [J_1 \ J_2]$, where J_1 and J_2 are given by:

$$J_1 = \begin{pmatrix} -\cos(\delta_{fl}) & -\cos(\delta_{fr}) & -1 & -1 \\ -\sin(\delta_{fl}) & -\sin(\delta_{fr}) & 0 & 0 \\ -L_f \sin(\delta_{fl}) + E/2 \cos(\delta_{fl}) & -L_f \sin(\delta_{fr}) - E/2 \cos(\delta_{fr}) & E/2 & -E/2 \\ R_{eff} & 0 & 0 & 0 \\ 0 & R_{eff} & 0 & 0 \\ 0 & 0 & R_{eff} & 0 \\ 0 & 0 & 0 & R_{eff} \end{pmatrix}, \quad (10)$$

$$J_2 = \begin{pmatrix} \sin(\delta_{fl}) & \sin(\delta_{fr}) & 0 & 0 & 1 \\ -\cos(\delta_{fl}) & -\cos(\delta_{fr}) & -1 & -1 & 0 \\ -L_f \cos(\delta_{fl}) - E/2 \sin(\delta_{fl}) & -L_f \cos(\delta_{fr}) + E/2 \sin(\delta_{fr}) & L_r & L_r & 0 \\ 0 & 0 & 0 & 0 & 0 \\ 0 & 0 & 0 & 0 & 0 \\ 0 & 0 & 0 & 0 & 0 \end{pmatrix}, \quad (11)$$

The vectors τ and f_e are given by:

$$\tau^t = (0 \ 0 \ 0 \ \tau_{w_{fl}} \ \tau_{w_{fr}} \ \tau_{w_{rl}} \ \tau_{w_{rr}}), \quad (12)$$

$$f_e^t = (F_{x_{fl}} F_{x_{fr}} F_{x_{rl}} F_{x_{rr}} F_{y_{fl}} F_{y_{fr}} F_{y_{rl}} F_{y_{rr}} F_{aero}) \quad (13)$$

The terms in L_3 and I_3 in (8) and (9) represent the interconnection between the different bodies composing the vehicle. Their presence makes the robotic approach more interesting, since it permits to develop a complete model of the vehicle showing the influence of each body on the other bodies. L_3 and I_3 are defined as

$$\begin{aligned} L_3 &= L_r(m_{rr} + m_{rl}) - L_f(m_{fl} + m_{fr}) \\ I_3 &= I_z + t_f^2(m_{rl} + m_{rr} + m_{fr} + m_{fl}) \\ &\quad + L_f^2(m_{fl} + m_{fr}) + L_r^2(m_{rr} + m_{rl}) \end{aligned} \quad (14)$$

The parameters m and I_z represent the vehicle mass and the moment of inertia around the z axis while L_f and L_r are the distances between the center of gravity and the front and the rear axles respectively. R_{eff} is the tire effective radius, I_w is the rotational inertia of the wheel and E is the vehicle track. $F_{x_{ij}}$ and $F_{y_{ij}}$ are the longitudinal and the lateral forces developed on the four wheels respectively, m_{ij} is the mass of a wheel, δ_{fl} and δ_{fr} are the front left and the front right steering wheel angles and $\tau_{w_{ij}}$ is the driving/braking torque applied to the wheel with index (ij).

C. Model Validation Results

The developed model is implemented under Matlab/Simulink. The model inputs are the steering angle δ and the wheels Driving/Braking torques $\tau_{w_{ij}}$, while the model outputs are the vehicle speeds in the longitudinal and the lateral directions, the yaw rate and the wheels angular velocities as well as the derivatives of these variables. To validate the developed model, we make use of a simulation environment: Scaner-Studio simulator [32].

Remark: It is suited that a validation of the proposed model using both real-time simulation (Scaner-Studio) and a real vehicle experiment's data is necessary to indicate the degree of confidence attributed to the validation using Scaner-Studio Simulator. However, the experimental vehicles present in the Heudiasyc laboratory are not equipped with a sensor that can measure the Driving/Braking torques applied to the wheels. And since this variable is one of the developed model inputs, a validation using experimental data is not executed.

Many simulations using the Scaner-Studio simulator were executed. In this simulator, we have used the autonomous driving mode. The reference trajectory was chosen among the predefined trajectories in the simulator and a desired speed profile was provided by the user.

The model inputs, δ and $\tau_{w_{ij}}$, are taken from the scenarios conducted on Scaner-Studio. These inputs were applied to the developed vehicle model under Matlab/Simulink. The obtained model outputs, which are the vehicle dynamic variables such as the speeds and the accelerations, are compared to the outputs obtained by the simulator.

Several scenarios that validate the model were executed. In [33], two scenarios validating the model are presented. The first one validates the longitudinal dynamics of the vehicle while the second validates the longitudinal and the lateral dynamics at relatively low speed.

In this paper, we present another scenario that validates the longitudinal and the lateral coupled vehicle dynamics at a respectively high speed.

The vehicle parameters are:

$$\begin{aligned} m_{ij} &= 20kg, \ m = 1744.6kg, \ \rho_a = 1.3kg/m^3 \\ s &= 3m^2, \ c_d = 0.63, \ h = 0.501m, \ g = 9.8m/s^2 \end{aligned}$$

$$Iz = 3015kg.m^2, \ L_f = 1.207m, \ L_r = 1.543m \quad (15)$$

$$I_w = 1.062kg.m^2, \ E = 1.492m$$

$$R_{eff} = 0.35m, \ \mu = 1.$$

The Dugoff's model [34] parameters are provided by the Scaner-Studio simulator as:

$$\begin{aligned} C_{\alpha_f} &= C_{\alpha_{fr}} = C_{\alpha_{fl}} = 65292N/rad \\ C_{\alpha_r} &= C_{\alpha_{rr}} = C_{\alpha_{rl}} = 67177N/rad \\ C_{\sigma_f} &= C_{\sigma_{fr}} = C_{\sigma_{fl}} = 82738N/rad \\ C_{\sigma_r} &= C_{\sigma_{rr}} = C_{\sigma_{rl}} = 85184N/rad \end{aligned} \quad (16)$$

where $C_{\alpha_{ij}}$ and $C_{\sigma_{ij}}$ represent the cornering and the longitudinal stiffness of the wheel ij .

Note that, the vehicle inputs are reduced to one steering angle on the front wheels, $\delta = \delta_{fr} = \delta_{fl}$, a front torque, $\tau_f = \tau_{w_{fl}} + \tau_{w_{fr}}$ and a rear torque $\tau_r = \tau_{w_{rl}} + \tau_{w_{rr}}$.

The model inputs are shown in Fig. 3 while the model outputs are given in Fig. 4. The vehicle speed varies between 15 and $25 m/s^2$ (54 to 90 km/h) and the steering angle goes from -8° to 2° . Observing Fig. 4, we can remark that the model outputs are very close to the outputs given by the Scaner-Studio model and this validates our developed model even when executing roundabouts with a high speed.

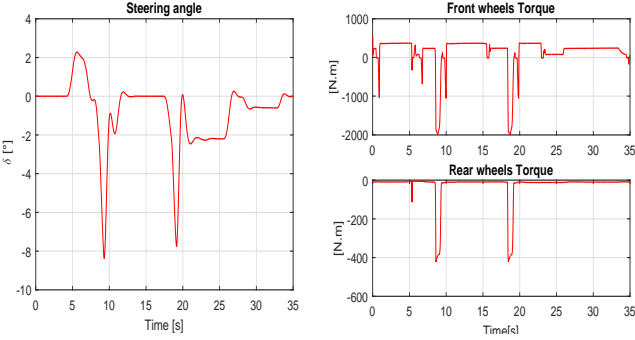


Fig. 3: Model inputs: Steering angle and wheels torques.

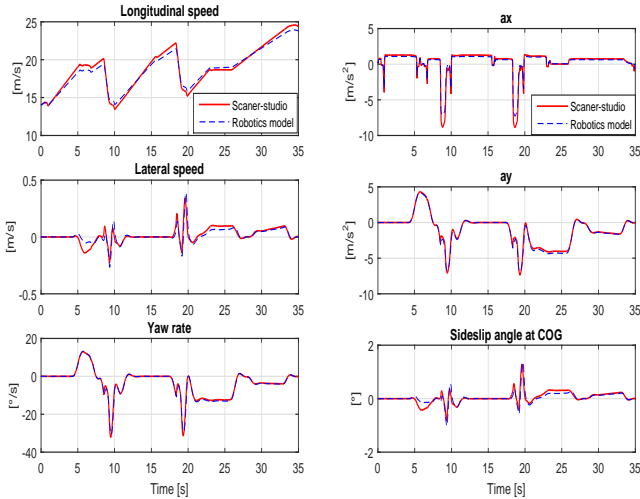


Fig. 4: Model outputs: Speeds, accelerations, yaw rate and sideslip angle.

To conclude this section, we note that the developed model is valid in a large marge of driving conditions and can be used for control objectives.

The next section of this paper presents the coupled controllers designed based on this model. The controller theory is explained in detail and we present, furthermore, the validation results.

III. VEHICLE CONTROL

A. Vehicle Model Simplification

The developed model presented in the second section is used here to accomplish the control objectives.

However, in order to simplify the controllers design task, the developed model was simplified using some usual assumptions :

- The estimation of the contact forces between the ground and the tires is based on the linear model.
- The approximation of small angles is made.
- The front left and the front right wheel's steering angles are supposed to be equal ($\delta_{fl} = \delta_{fr} = \delta$).
- The longitudinal slip ratio is considered approximately null, that renders:

$$R_{eff} w_{ij} = \dot{x}. \quad (17)$$

where $\omega_{ij} = \dot{\theta}_{ij}$ represent the angular speed of the wheel ij . The dynamic equation of the wheel ij can be written in the following form (from (7)) :

$$I_w \ddot{w}_{ij} = \tau_{ij} - R_{eff} F_{x_{ij}}. \quad (18)$$

Using (17) and (18), we can find:

$$F_{x_{ij}} = \frac{\tau_{w_{ij}}}{R_{eff}} - \frac{I_w \ddot{x}}{R_{eff}^2}. \quad (19)$$

Integrating (19) in the first equation of (7), we obtain:

$$\begin{aligned} m \ddot{x} - m \dot{y} \dot{\psi} + L_3 \dot{\psi}^2 + F_{aero} - \frac{\tau_w}{R_{eff}} + 4 \frac{I_w \ddot{x}}{R_{eff}^2} \\ + \delta (F_{y_{fl}} + F_{y_{fr}}) = 0. \end{aligned} \quad (20)$$

where $\tau_w = \sum \tau_{w_{ij}}$ is the total Driving/Braking torque applied on the four wheels of the vehicle.

- Integrating (19) in the second equation of (7) and introducing the linear model to estimate the lateral forces at the contact ground/tires, we have:

$$\begin{aligned} m \ddot{y} + m \dot{x} \dot{\psi} + 2C_{\alpha_f} \frac{\dot{x}(\dot{y} + L_f \dot{\psi})}{\dot{x}^2 - (t_f \dot{\psi})^2} + 2C_{\alpha_r} \frac{\dot{x}(\dot{y} - L_r \dot{\psi})}{\dot{x}^2 - (t_f \dot{\psi})^2} \\ - L_3 \ddot{\psi} = (2C_{\alpha_f} - 2 \frac{I_w}{R_{eff}^2} \ddot{x} + \frac{\tau_{w_{fl}} + \tau_{w_{fr}}}{R_{eff}}) \delta, \end{aligned} \quad (21)$$

We consider that the torque doesn't influence the lateral dynamics, and we neglect the term $\delta \frac{\tau_{w_{fl}} + \tau_{w_{fr}}}{R_{eff}}$. Indeed, the cornering stiffness of the front wheels is much greater than the maximal admissible torque. We saturate the torque to 1000 N.m on each wheel while the cornering stiffness is $C_{\alpha_f} = 65292$ N/rad, hence $2C_{\alpha_f} >> \frac{\tau_{w_{fl}} + \tau_{w_{fr}}}{R_{eff}}$.

With all these assumptions, the vehicle model presented in (7) can be rewritten as:

$$\begin{aligned} m_e \ddot{x} - m \dot{y} \dot{\psi} + L_3 \dot{\psi}^2 + F_{aero} = g_1, \\ m \ddot{y} + m \dot{x} \dot{\psi} - L_3 \ddot{\psi} + 2C_{\alpha_f} \frac{\dot{x}(\dot{y} + L_f \dot{\psi})}{\dot{x}^2 - (t_f \dot{\psi})^2} + 2C_{\alpha_r} \frac{\dot{x}(\dot{y} - L_r \dot{\psi})}{\dot{x}^2 - (t_f \dot{\psi})^2} = g_2, \\ I_3 \ddot{\psi} + 2L_f C_{\alpha_f} \frac{\dot{x}(\dot{y} + L_f \dot{\psi})}{\dot{x}^2 - (t_f \dot{\psi})^2} - 2L_r C_{\alpha_r} \frac{\dot{x}(\dot{y} - L_r \dot{\psi})}{\dot{x}^2 - (t_f \dot{\psi})^2} = g_3, \end{aligned} \quad (22)$$

where m_e, g_1, g_2 and g_3 are given by:

$$\begin{aligned} m_e &= m + 4 \frac{I_w}{R_{eff}^2}, \\ g_1 &= \frac{\tau_w}{R_{eff}} - \delta (2C_{\alpha_f} \delta - 2C_{\alpha_f} \frac{\dot{x}(\dot{y} + L_f \dot{\psi})}{\dot{x}^2 - (t_f \dot{\psi})^2}) \\ g_2 &= (2C_{\alpha_f} - 2 \frac{I_w}{R_{eff}^2} \ddot{x}) \delta, \\ g_3 &= L_f g_2 + (-t_f C_{\alpha_f} \frac{2t_f \dot{\psi}(\dot{y} + L_f \dot{\psi})}{\dot{x}^2 - (t_f \dot{\psi})^2}) \delta + L_3 (\dot{y} + \dot{x} \dot{\psi}). \end{aligned} \quad (23)$$

C_{α_f} and C_{α_r} are the cornering stiffness of the front and the rear wheels.

B. Coupled Controllers design

1) Problem Formulation:

In this work, we aim to propose some vehicle controllers that can handle its safety and stability, by taking into account the strong coupling between the vehicle's longitudinal and lateral dynamics. Indeed, the objective of our controllers is to ensure a robust tracking of the reference trajectory for any time varying maneuver. This objective is reached by controlling the longitudinal velocity and the lateral displacement of the vehicle in order to track a desired longitudinal speed while canceling the lateral displacement error with respect to a given reference trajectory. The control inputs are the steering wheel angle, δ , and the Driving/Braking wheels torque, τ_w (see Fig. 5).

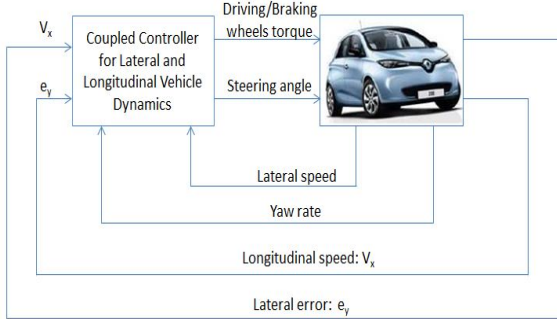


Fig. 5: Vehicle control layout.

2) Lyapunov Based Controller:

As mentioned above, the controller role is to guarantee a robust tracking of the reference trajectory for any time varying maneuver. Thus, the controller computes the Driving/Braking torque (τ_w) necessary to drive at a given desired speed, and, the steering wheel angle that will cancel the lateral displacement error with respect to a given reference trajectory.

To accomplish the control objective, we define two error signals as:

$$s_1 = \dot{e}_{y_f} + \lambda_y e_{y_f}, \quad \lambda_y > 0 \quad (24)$$

$$s_2 = e_{vx} + \lambda_x \int e_{vx}, \quad \lambda_x > 0 \quad (25)$$

where s_1 is a function of the lateral displacement error (e_{y_f}) and its derivative, and s_2 is a function of the vehicle longitudinal speed error $e_{vx} = \dot{x} - \dot{x}^*$ and its integral. The vectors with superscript (*) represent desired outputs.

The lateral displacement error e_{y_f} is computed at a look-ahead distance L_s from the center of gravity of the vehicle (see Figure 6), in order to take into account the delay of the controllers/actuators. This parameter should be adapted to the vehicle speed and the trajectory curvature as follows: When

the vehicle speed increases, L_s should increase. And when the trajectory curvature increases, L_s should decrease.

e_{y_f} is then given by:

$$e_{y_f} = e_y + L_s e_\psi. \quad (26)$$

where e_y is the lateral displacement error computed at the vehicle's center of gravity and e_ψ is the yaw angle error with respect to the reference trajectory.

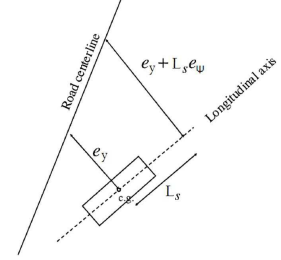


Fig. 6: Lateral displacement error computed at a distance L_s in front of the vehicle

Assuming that the desired lateral acceleration of the vehicle on the reference trajectory can be written as [16]:

$$a_y^* = \dot{x}^2 \rho_{ref}, \quad (27)$$

where ρ_{ref} is the reference trajectory curvature, and given that the lateral acceleration in a fixed frame is $a_y = \ddot{y} + \dot{x}\dot{\psi}$, we have:

$$\ddot{e}_y = a_y - a_y^* = \ddot{y} + \dot{x}\dot{\psi} - \dot{x}^2 \rho_{ref} \quad (28)$$

The trajectory tracking is then guaranteed if and only if s_1 and s_2 converge to zero.

In this first controller, we make use of the Lyapunov control concept to deduce the suitable control laws. Indeed, the control strategy proposed in this work provides an algorithm to design in one step a nonlinear controller dealing with both the longitudinal and the lateral dynamics of the vehicle.

We define then a Lyapunov function as:

$$V = \frac{1}{2}s_1^2 + \frac{1}{2}\gamma s_2^2, \quad \gamma > 0 \quad (29)$$

To ensure an exponential convergence of s_1 and s_2 , which guarantees the convergence of e_y , \dot{e}_y and e_{vx} , we impose a negative variation of V as:

$$\begin{aligned} \dot{V} &= s_1 \dot{s}_1 + \gamma s_2 \dot{s}_2 \\ &= -K_{lyy} s_1^2 - \gamma K_{lyx} s_2^2 \end{aligned} \quad (30)$$

where K_{lyx} and K_{lyy} represent the positive gains of the controller.

The condition (30) can be satisfied by taking:

$$s_1 \dot{s}_1 = -K_{lyy} s_1^2 \implies s_1 = -K_{lyy} s_1. \quad (31)$$

$$s_2 \dot{s}_2 = -K_{lyx} s_2^2 \implies s_2 = -K_{lyx} s_2. \quad (32)$$

Integrating (24) and (25) into (31) and (32), we obtain:

$$\ddot{e}_{y_f} = -(K_{lyy} + \lambda_y)\dot{e}_{y_f} - K_{lyy}\lambda_y e_{y_f}. \quad (33)$$

$$\ddot{x} = \ddot{x}^* - (K_{lyx} + \lambda_x)e_{vx} - K_{lyx}\lambda_x \int e_{vx}. \quad (34)$$

From (28), (26) and (33), we have:

$$\ddot{y} = \dot{x}^2 \rho_{ref} - \dot{x}\dot{\psi} - (K_{lyy} + \lambda_y)\dot{e}_{y_f} - K_{lyy}\lambda_y e_{y_f} - L_s \ddot{e}_\psi. \quad (35)$$

By replacing (34) and (35) in the reduced system (22), we can deduce the longitudinal and the lateral controls as follows:

$$\begin{aligned} \tau_w = & R_{eff}[m_e \ddot{x}^* - m_e(K_{lyx} + \lambda_x)e_{vx} - m_e K_{lyx}\lambda_x \int e_{vx} \\ & - m\dot{y}\dot{\psi} + L_3\dot{\psi}^2 + \delta(2C_{\alpha_f}\delta - 2C_{\alpha_f} \frac{\dot{x}(\dot{y} + L_f\dot{\psi})}{\dot{x}^2 - (\frac{E}{2}\dot{\psi})^2}) + F_{aero}] \end{aligned} \quad (36)$$

$$\begin{aligned} \delta = & \frac{1}{(2C_{\alpha_f} - 2\frac{I_w}{R_{eff}^2}\ddot{x})} [m\dot{x}^2 \rho_{ref} - mL_s \ddot{e}_\psi - L_3 \ddot{\psi} \\ & - mK_{lyy}\lambda_y e_{y_f} + 2C_{\alpha_f} \frac{\dot{x}(\dot{y} + L_f\dot{\psi})}{\dot{x}^2 - (\frac{E}{2}\dot{\psi})^2} \\ & - m(K_{lyy} + \lambda_y)\dot{e}_{y_f} + 2C_{\alpha_r} \frac{\dot{x}(\dot{y} - L_r\dot{\psi})}{\dot{x}^2 - (\frac{E}{2}\dot{\psi})^2}], \end{aligned} \quad (37)$$

3) I&I Based Controller:

The immersion and invariance approach is a relatively recent method for designing nonlinear and adaptive controllers [35]. This method uses the notions of immersion and invariance to ensure the objective of the command. Indeed, the idea of this method consists in immersing the dynamics of the system in a target dynamic that ensures the desired behavior. This is done by finding a manifold in the state space that can be made invariant and attractive - with an internal dynamic which reflects the dynamics of the closed loop system (see Fig. 7). In other words, the Immersion and Invariance (I & I) theory consists of defining a target dynamics and to design a control law that makes the target dynamic attractive and invariant. The advantage of such an approach is to reduce the problem of the controller design into a sub-problem that could be more easily solved.

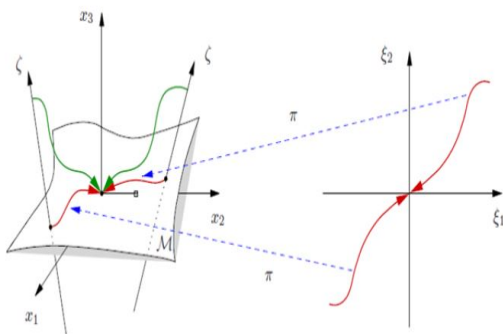


Fig. 7: Principle of the Immersion and Invariance control [35].

Using the fact that the lateral dynamics converge faster than the longitudinal dynamics of the vehicle, we define the manifold as the equilibrium surface of the lateral dynamics, that is $s_1 = \dot{e}_{y_f} + \lambda_y e_{y_f} = 0$ (see Fig.8).

In order to reach this manifold, the objective is to converge the “off-the-manifold” variable s_1 to zero. A sliding mode control (SMC) approach [36] is then used to control the “off-the-manifold” variable. The objective is then to define a suitable steering wheel angle that can guide the vehicle to the defined manifold. Once the manifold is reached, the stabilisation of the longitudinal dynamics is considered inside the manifold corresponding to $s_1 = 0$. This means that, at this level, the lateral dynamic variables have converged to their equilibrium states. A Lyapunov controller is then used, at this level, in order to reach the desired longitudinal speed.

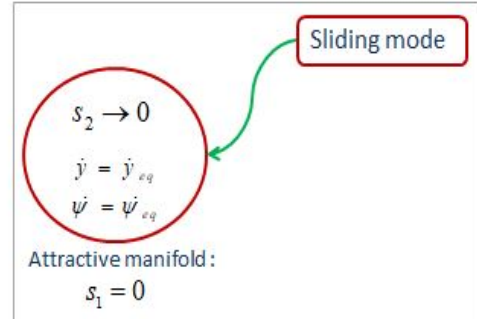


Fig. 8: Principle of the I&I vehicle controller.

Indeed, the SMC approach has been developed since the 1950s and is recognized as one of the most promising techniques for robust control. The idea is to define a sliding surface that represents the desired dynamic state of the system and then constrain the system in order to reach the sliding surface in a finite time and remain on it (see Fig. 9).

Using the sliding mode control, only the measurement of the sliding variable in real time is required to deduce a robust control law. However, the discontinuities in the control law can cause a phenomenon of chatter, called, “chattering”. This is characterized by strong oscillations of the trajectories of the system around the sliding surface. Many methods can be used to reduce the chattering impact. In this work, we choose to proceed with a higher order sliding mode (second order) based on the super-twisting algorithm. This algorithm is developed to control systems with a relative degree 1, and to ensure robust stability while reducing chattering.

Consider a system of the form:

$$\dot{X} = f(t, X) + g(t, X)u(t) \quad (38)$$

where u is the control input, $X \in R^n$ is the state vector, and, f and g are continuous functions.

We define a sliding variable s of relative degree 1, whose derivative can be expressed as follows:

$$\dot{s}(t, s) = \phi(t, s) + \varphi(t, s)u(t) \quad (39)$$

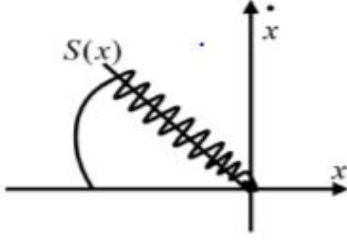


Fig. 9: Sliding mode principle [37].

The controller aims to ensure the system convergence to the sliding surface defined by $s = 0$.

It is assumed that there exist positive constants s_0, b_{min}, b_{max} and C_0 such that $\forall x \in R^n$ and $|s(t, x)| < s_0$, the system satisfies the following conditions:

$$\begin{cases} |u(t)| \leq U_{max} \\ 0 < b_{min} \leq \varphi(t, s) \leq b_{max} \\ |\phi(t, s)| < C_0 \end{cases} \quad (40)$$

The super-twisting sliding mode control input is then given by:

$$u(t) = u_1 + u_2 \begin{cases} u_1 = -\alpha|s|^{\tau} sign(s), \tau \in]0, 0.5] \\ \dot{u}_2 = -\beta sign(s) \end{cases} \quad (41)$$

with α and β positive constants.

The finite time convergence to the sliding surface is guaranteed by the following conditions:

$$\begin{cases} \beta > \frac{C_0}{b_{min}} \\ \alpha \geq \sqrt{\frac{4C_0(b_{max}\beta + C_0)}{b_{min}^2(b_{min}\beta - C_0)}} \end{cases} \quad (42)$$

For more details of the convergence and robustness of the super-twisting algorithm, see [38], [39].

To apply this control technique to the vehicle lateral dynamic system, we define the sliding surface by the off-the-manifold variable s_1 given by (24) as:

$$s_1 = \dot{e}_{y_f} + \lambda_y e_{y_f}, \lambda_y > 0 \quad (43)$$

Note that the lateral dynamics of the vehicle given by the second equation of (22) can be written in the form of (38) where:

$$\begin{aligned} X &= \dot{y} \\ u(t) &= \delta \\ f(t, X) &= -\dot{x}\psi + \frac{L_3}{m}\ddot{\psi} - 2\frac{C_{\alpha_f}}{m}\frac{\dot{x}(\dot{y} + L_f\dot{\psi})}{\dot{x}^2 - (t_f\dot{\psi})^2} \\ &\quad - 2\frac{C_{\alpha_r}}{m}\frac{\dot{x}(\dot{y} - L_r\dot{\psi})}{\dot{x}^2 - (t_f\dot{\psi})^2} \\ g(t, X) &= \frac{1}{m}(2C_{\alpha_f} - 2\frac{I_w}{R_{eff}^2}\ddot{x}) \end{aligned} \quad (44)$$

Using (28), (24), (26) and (22), we can find:

$$\begin{aligned} \dot{s}_1 &= \frac{1}{m}(L_3\ddot{\psi} - 2C_{\alpha_f}\frac{\dot{x}(\dot{y} + L_f\dot{\psi})}{\dot{x}^2 - (\frac{E}{2}\dot{\psi})^2} - 2C_{\alpha_r}\frac{\dot{x}(\dot{y} - L_r\dot{\psi})}{\dot{x}^2 - (\frac{E}{2}\dot{\psi})^2} \\ &\quad + (2C_{\alpha_f} - 2\frac{I_w}{R_{eff}^2}\ddot{x})\delta) - \dot{x}^2\rho_{ref} + L_s\ddot{e}_{\psi} + \lambda_y\dot{e}_{y_f}. \end{aligned} \quad (45)$$

Note that the relative degree ($\delta \rightarrow s_1$) is one. By identification with (39), we have:

$$\dot{s}_1(t, s_1) = \phi(t, s_1) + \varphi(t, s_1)\delta, \text{ with:}$$

$$\left\{ \begin{array}{l} \phi(t, s_1) = \frac{1}{m}(-2C_{\alpha_f}\frac{\dot{x}(\dot{y} + L_f\dot{\psi})}{\dot{x}^2 - (\frac{E}{2}\dot{\psi})^2} - 2C_{\alpha_r}\frac{\dot{x}(\dot{y} - L_r\dot{\psi})}{\dot{x}^2 - (\frac{E}{2}\dot{\psi})^2}) \\ \quad + \frac{L_3}{m}\ddot{\psi} - \dot{x}^2\rho_{ref} + \lambda_y\dot{e}_{y_f} + L_s\ddot{e}_{\psi} \\ \varphi(t, s_1) = \frac{1}{m}(2C_{\alpha_f} - 2\frac{I_w}{R_{eff}^2}\ddot{x}) \end{array} \right.$$

Applying the super-twisting theorem, the control input can be defined as follows:

$$u(t) = u_1 + u_2 \begin{cases} u_1 = -\alpha|s_1|^{0.5} sign(s_1) \\ u_2 = -\beta sign(s_1) \end{cases} \quad (46)$$

Finally, an equivalent command δ_{eqvl} , corresponding to the steering wheels angle when $\dot{s}_1 = 0$, is added as a feed forward that approaches the system to the sliding surface. This term is given by (45):

$$\begin{aligned} \delta_{eqvl} &= \frac{1}{(2C_{\alpha_f} - 2\frac{I_w}{R_{eff}^2}\ddot{x})(-L_3\ddot{\psi} + 2C_{\alpha_f}\frac{\dot{x}(\dot{y} + L_f\dot{\psi})}{\dot{x}^2 - (\frac{E}{2}\dot{\psi})^2} \\ &\quad + 2C_{\alpha_r}\frac{\dot{x}(\dot{y} - L_r\dot{\psi})}{\dot{x}^2 - (\frac{E}{2}\dot{\psi})^2} + m\dot{x}^2\rho_{ref} - m\lambda_y\dot{e}_{y_f} - mL_s\ddot{e}_{\psi}). \end{aligned} \quad (47)$$

Hence, the steering angle representing the control input of the system is defined as follows:

$$\delta = u_1 + u_2 + \delta_{eqvl} \quad (48)$$

Once the manifold is reached, we proceed to stabilize the longitudinal dynamics inside the manifold corresponding to $s_1 = 0$. At this level, we consider that the lateral dynamic variables have converged to their equilibrium states. In other words, $\dot{y} = \dot{y}_{eq}$, $\dot{\psi} = \dot{\psi}_{eq}$ and $\delta = \delta_{eq}$, where:

$$\begin{aligned} \dot{\psi}_{eq} &\triangleq \rho_{ref}\dot{x} \\ \dot{y}_{eq} &\triangleq L_r\dot{\psi}_{eq} - \frac{mL_f + L_3}{2(L_f + L_r)C_{\alpha_f}}\dot{\psi}_{eq}\dot{x}^2 \\ \delta_{eq} &\triangleq \frac{1}{2L_f C_{\alpha_f}\dot{x}}[(2L_f C_{\alpha_f} - 2L_r C_{\alpha_r})\dot{y}_{eq} + 2L_f^2 C_{\alpha_f}\dot{\psi}_{eq} \\ &\quad + 2L_r^2 C_{\alpha_r}\dot{\psi}_{eq} - L_3\dot{x}^2\dot{\psi}_{eq}] \end{aligned} \quad (49)$$

The convergence of the longitudinal dynamics inside the manifold is then assured by the use of a Lyapunov function defined as follows:

$$V = \frac{1}{2}s_2^2. \quad (50)$$

In order to ensure the convergence of the longitudinal speed, we impose a negative variation of the function V, as follows:

$$\begin{aligned}\dot{V} &= s_2 \dot{s}_2 \\ &= -K_{imx} s_2^2\end{aligned}\quad (51)$$

where K_{imx} is a positive constant.

This yields:

$$\begin{aligned}\dot{s}_2 &= -K_{imx} s_2 \\ \dot{e}_{vx} + \lambda_x e_{vx} &= -K_{imx}(e_{vx} + \lambda_x) \int e_{vx}\end{aligned}\quad (52)$$

Replacing e_{vx} by $\dot{x} - \dot{x}^*$, we obtain:

$$\ddot{x} = \ddot{x}^* - (K_{imx} + \lambda_x)e_{vx} - K_{imx}\lambda_x \int e_{vx} \quad (53)$$

Using (53) and (22) and replacing the lateral variables by their equilibrium states, we deduce the Driving/Braking wheels torque as:

$$\begin{aligned}\tau_w &= R_{eff}[m_e \ddot{x}^* - m_e(K_{imx} + \lambda_x)e_{vx} - m_e K_{imx} \lambda_x \int e_{vx} \\ &\quad - m \dot{y}_{eq} \dot{\psi}_{eq} + \delta_{eq}(2C_{\alpha_f} \delta_{eq} - 2C_{\alpha_f} \frac{\dot{x}(\dot{y}_{eq} + L_f \dot{\psi}_{eq})}{\dot{x}^2 - (\frac{E}{2} \dot{\psi}_{eq})^2}) \\ &\quad + L_3 \dot{\psi}_{eq}^2 + F_{aero}]\end{aligned}\quad (54)$$

IV. CONTROLLERS VALIDATION

The coupled vehicle controllers were validated firstly by simulation under Matlab/Simulink and then experimentally using a robotized vehicle. We present in this section some validation results.

Remark: The autonomous navigation requires three main steps: the perception, the trajectory planning and the vehicle control. We consider in this work, treating the vehicle control problem, that the desired trajectory and the desired speed are generated in the trajectory planning level. Thus, it is the duty of this higher level to provide the vehicle controller with a safe trajectory that can be tracked in the limits of stability of the vehicle. The reader can refer to our work on the trajectory planning in [40] and [41].

In our work, we just check if the speed profile can be safely executed according to the curvature of the given trajectory, using the definition presented in [15]:

$$V_{max} = \sqrt{\frac{g\mu}{\rho_r}} \quad (55)$$

where V_{max} is the maximum longitudinal safe speed considering the road curvature; g , μ and ρ_r are respectively the gravity, the friction coefficient and the road curvature.

A. Controllers Validation by Simulation

To validate our control laws by simulation, we make use of the real experimental data collected by performing several tests on the vehicle DYNA (Peugeot 308 sw) present in the Heudiasyc laboratory. The tests were conducted on the track CERAM ("Centre d'Essais et de Recherche Automobile de Mortefontaine").



Fig. 10: Experimental vehicle DYNA and the track CERAM

The experimental vehicle and the track CERAM are shown in Fig. 10.

Remark: The validation of the controllers shown in this paragraph is done under Matlab/Simulink using real experimental data. We note that, a co-simulation between Matlab/Simulink and Scaner-Studio was very suited, since the simulator presents the possibility of testing different scenarios in different driving conditions and this permits to test the robustness of the controllers while executing lane-change maneuvers, obstacle avoidance maneuvers and combined maneuvers in critical driving situations. This objective wasn't achieved since the control inputs computed by the developed controllers are the steering wheel angle and the Driving/Braking wheels torques while the control inputs of the Scaner-Studio vehicle model are the steering wheel angle and the force that should be applied on the accelerator pedal. This means that a new level transforming the wheels torques into the accelerator force is needed. And since the transmission chain between the accelerator pedals and the wheels is not given under Scaner-Studio, we couldn't configure this level.

The validation of the coupled controllers is schematized in Fig. 11. The vehicle speed profiles executed in these tests are considered as the desired speed in the simulation. The reference trajectory curvature is used to calculate the lateral displacement error as in (28). The desired speed and the lateral displacement error are then used to compute the control inputs, the Driving/Braking torque and the steering wheel angle, using a selected controller among the developed controllers. The control inputs are then transmitted to the vehicle model that computes the vehicle dynamic variables. We compare finally these variables, namely the lateral acceleration and the yaw rate, to their corresponding experimental values. The steering wheel angle computed by the controllers is also compared to the experimental variable in order to evaluate the compatibility of the controllers.

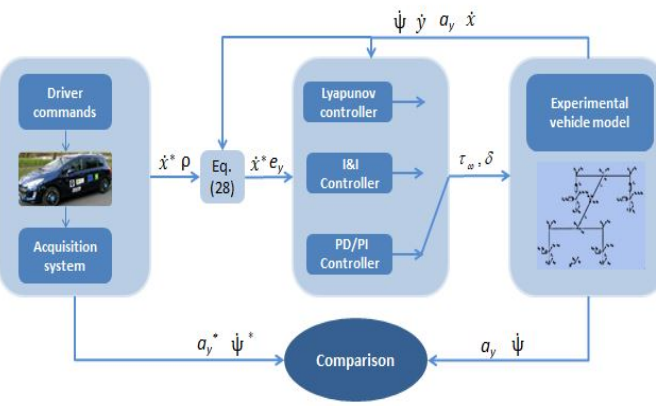


Fig. 11: Coupled Controllers validation schema.

The vehicle and the aerodynamic parameters are as follows:

$$\begin{aligned}
 m_{ij} &= 12.2\text{kg}, \quad m = 1719\text{kg}, \quad \rho_a = 1.3\text{kg/m}^3 \\
 s &= 2.31\text{m}^2, \quad c_d = 0.314, \quad g = 9.8\text{m/s}^2 \\
 I_z &= 3300\text{kg.m}^2, \quad L_f = 1.195\text{m}, \quad L_r = 1.513\text{m} \quad (56) \\
 C_{\alpha_r} &= 68922\text{N/rad}, \quad C_{\alpha_f} = 85275\text{N/rad}, \quad E = 1.4\text{m} \\
 R_{eff} &= 0.316\text{m}, \quad I_w = 1.02\text{kg.m}^2.
 \end{aligned}$$

For a further evaluation of the proposed controllers, a comparison with a classical PD/PI controller is made. The PD/PI control inputs are as follows:

$$\delta = -K_{dy}\dot{e}_{y_f} - K_{py}e_{y_f} \quad (57)$$

$$\tau_w = -K_{px}e_{vx} - K_{ix}\int e_{vx}, \quad (58)$$

where K_{dy} , K_{py} , K_{px} and K_{ix} are positive constants.

Several tests were done to evaluate the controllers performances during normal and critical driving conditions. The controllers robustness was also studied by considering the vehicle parameters uncertainties. In the following, some validation results and some conclusions are presented.

For the control laws, we used the following gains:

$$\begin{aligned}
 K_{lyx} &= 1, \quad K_{lyy} = 8, \quad K_{imx} = 1, \quad \alpha = 0.2, \quad \beta = 0.0001, \\
 \lambda_x &= 0.001, \quad \lambda_y = 8, \quad K_{px} = 436, \quad K_{ix} = 0.45, \quad K_{dy} = 0.7, \\
 K_{py} &= 1.
 \end{aligned}$$

Note that the choice of the controllers gains is done as follows: The range of the controller gains is set due to the vehicle dynamics analyses. We proceed then to tune these gains by simulation under Matlab/Simulink.

The parameter L_s introduced to compensate the lateral controllers/actuators delay is fixed to 3m. In fact, the delay between sending the steering wheel angle value computed by the controller and the execution of this angle is experimentally estimated by 80ms. In the simulations, the steering actuator is modeled by a first order low pass filter with a cut-off frequency of 10 Hz. This modeling induces a delay of 100ms that represents approximately the real steering actuator delay.

1) Normal Driving Conditions:

A normal driving scenario used to validate our controllers is presented in Fig. 12, Fig. 13 and 14. In this test, the longitudinal desired speed is almost 13m/s except on the roundabout, where the driver decelerates to reach near 7m/s. The lateral acceleration varies between -4m/s^2 and 4m/s^2 almost. Fig. 13b and Fig. 12 shows that the vehicle navigates with the desired speed while tracking the reference trajectory either with the I&I or the Lyapunov or the PD/PI based controllers. The comparison of the lateral acceleration, the yaw rate and the steering angle with the experimental data (Fig. 14b, Fig. 14d and Fig. 14c) shows that the controllers execute the desired trajectory profile in a similar way to the vehicle driver. The control inputs computed by the controllers are shown in Fig. 14c and Fig. 14a. However, in this normal driving scenario, the Lyapunov and the I&I based controllers present a lateral and a longitudinal error smaller than that provided by the PD/PI based one (Fig. 13d and Fig. 13b). Note that the error presented by the PD/PI controller is not risky in this scenario but it could be in different driving scenarios as it will be shown in the Controllers Experimental Validation section.

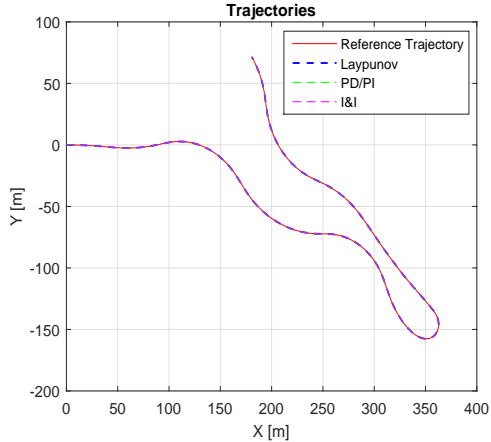


Fig. 12: Scenario 1: Reference and vehicle trajectory

The comparison between the Lyapunov based controller, the Immersion and Invariance controller and the PD/PI controller was done using several scenarios. The performances of these three controllers are similar to what is shown in this paragraph. The results suggest that the proposed coupled controllers (Lyapunov and I & I) are more performant in normal driving conditions than a classical PD/PI controller.

Note that the assumption of linear contact forces between the ground and the tires, considered in the controllers design, is not violated in this scenario. Fig. 15 shows that the lateral forces computed by the Linear model are approximately the same when computed with a non-linear model such as Dugoff's model.

2) Strongly Nonlinear Maneuvers:

The test presented in Fig. 16, Fig. 17 and Fig. 18 shows a highly nonlinear maneuver. It consists of increasing progressively the vehicle speed while executing a J-turn having a

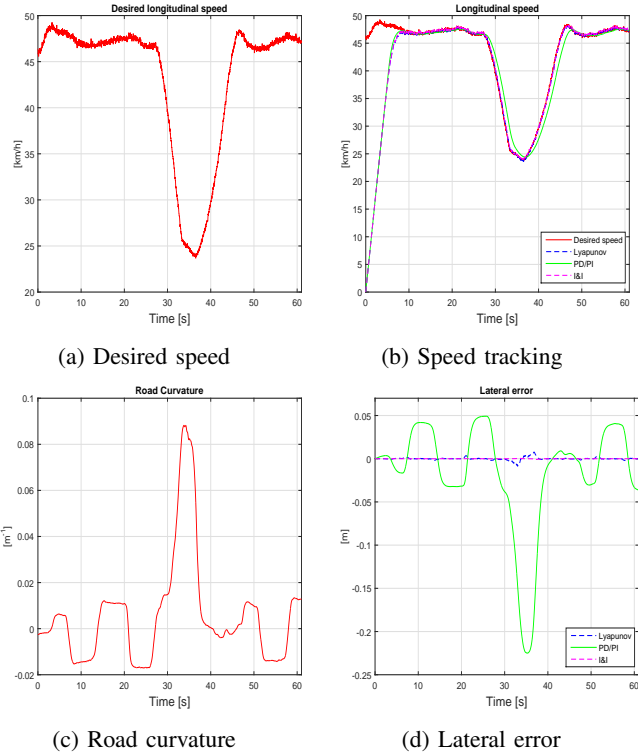


Fig. 13: Normal driving conditions, Scenario 1: Longitudinal speed and trajectory tracking

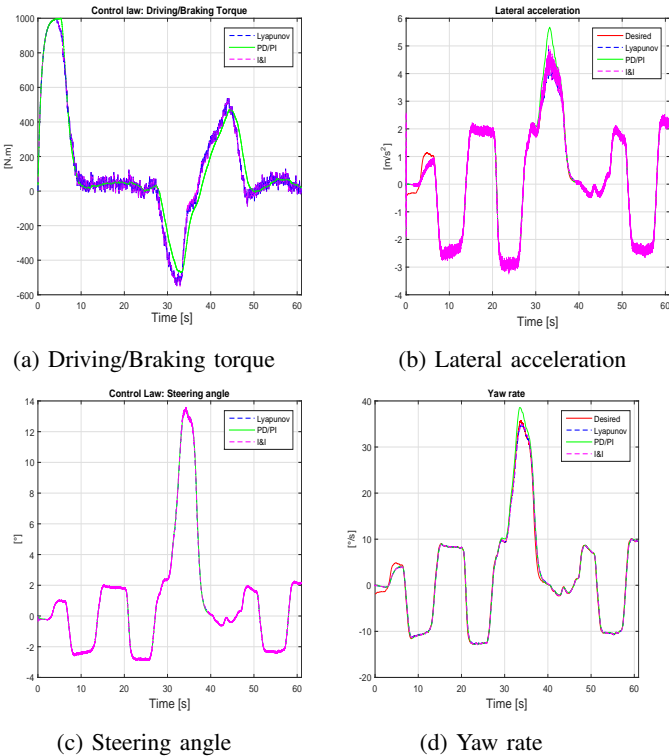


Fig. 14: Normal driving conditions, Scenario 1: Control laws and lateral dynamics.

radius of about 50m. The desired speed profile and the road curvature are presented in Fig. 17a and Fig. 17c. The reference trajectory tracking is shown in Fig. 16. The lateral acceleration

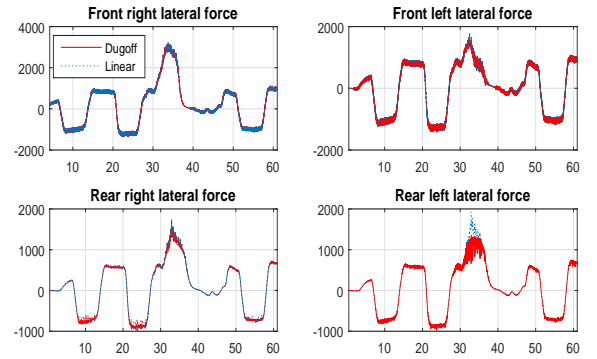


Fig. 15: Scenario 1: Lateral contact forces computed by Linear vs Dugoff's Tire forces model.

and the longitudinal speed are increasing remarkably (the speed is increasing with a rate of $1m/s^2$ and the lateral acceleration reaches $7.5m/s^2$). This type of test is used to evaluate the stability and the robustness of the controllers against strong nonlinear dynamics. Fig. 17b shows the speed profile tracking while Fig. 17d shows the lateral error displacement of the three controllers, the Lyapunov based controller, the *I&I* controller and the PD/PI controller.

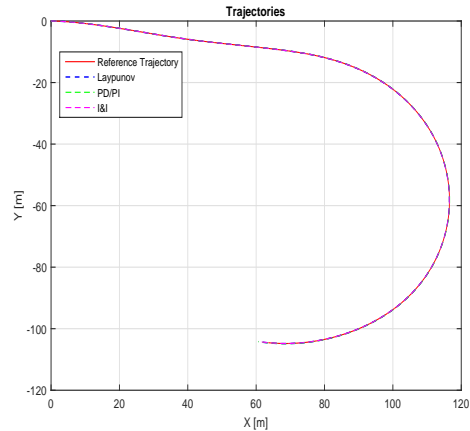


Fig. 16: Strongly nonlinear maneuver, Scenario 2: Reference and vehicle trajectories

In Figure 18b and Fig. 18d, the dynamic variables are compared to those measured on the vehicle (curves in red). Fig. 18c shows the steering wheel angle computed by the controllers with respect to that executed by the driver, while Fig. 18a shows the Driving/Braking wheels torque.

The PD/PI and the *I&I* controllers present almost the same behavior they have presented in normal driving conditions. The lateral error produced by the *I&I* controller is always very small and smaller than the lateral error produced by the PD/PI controller. However, the Lyapunov based controller performance is decreasing since the lateral error it produced is higher than that produced in normal driving conditions, even if it remains acceptable. By consequence, the *I&I* and the Lyapunov performances are better than that of the PD/PI based controller in critical driving scenarios where the vehicle approaches the limits of stability. However, the

Lyapunov based controller performance decreases at the limit of stability. This performance lost can be explained by the simplifications of the vehicle model (see III-A). Since the Lyapunov based controller depends on the vehicle model even to regulate the lateral dynamics and the longitudinal dynamics, the vehicle model used to derive its control laws must be very accurate, especially in critical driving situations. However, using a complete vehicle model to derive the control laws of the Lyapunov based controller increases the problem complexity. For example, the assumption of small angles doesn't hold when executing big roundabouts. This assumption violation was tested in scenario 1 but with normal driving conditions. When violating this assumption with high speed, the performance of the controller will be affected. Besides, in order to design our Lyapunov controller, we have modeled the contact forces between the wheels and the ground by a linear model. This model is not valid in critical driving scenarios. We can observe a clear difference between the lateral forces computed by the linear model and those computed by Dugoff's non-linear model in Fig. 19. Thus, the linear model should be replaced by a nonlinear model, such as Dugoff's model, piece-wise linear tire model and others. However, the use of a nonlinear tire model renders the derivation of the control laws more complex when using Lyapunov based control.

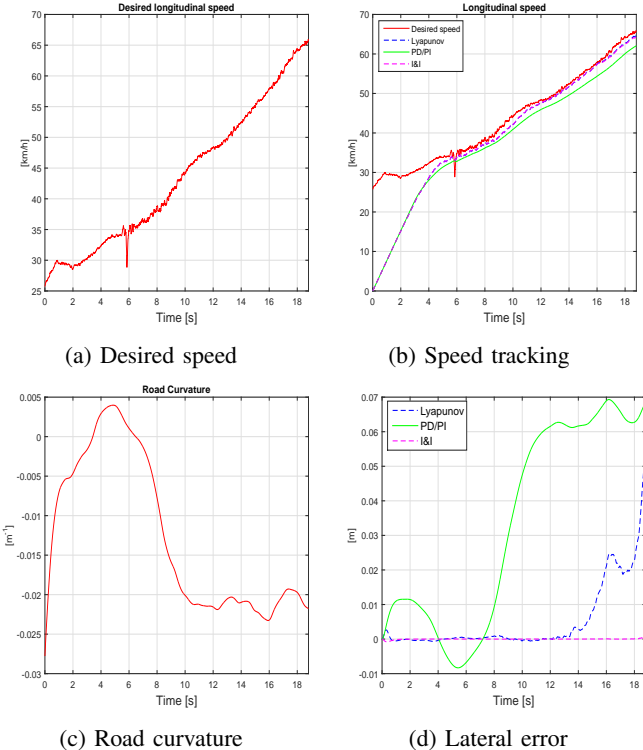


Fig. 17: Strongly nonlinear maneuver, Scenario 2: Longitudinal speed and trajectory tracking.

To conclude, we can claim that the developed controllers have good performances in normal and critical driving situations. In normal driving scenarios as in critical driving scenarios, the coupled controllers, the Lyapunov and the *I&I* based ones,

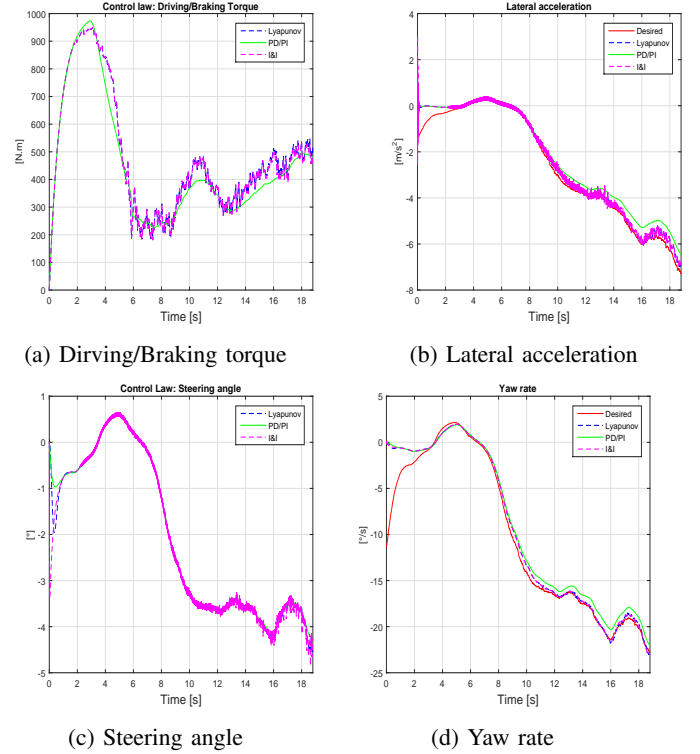


Fig. 18: Strongly nonlinear maneuver, Scenario 2: Control laws and lateral dynamics.

present better performances than a classical PD/PI controller.

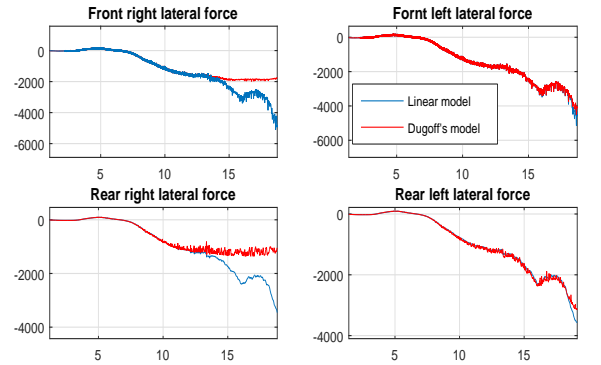


Fig. 19: Scenario 2: Lateral contact forces computed by Linear vs Dugoff's Tire forces model.

3) Robustness to Parameters Uncertainties: The robustness of the controllers is evaluated over the vehicle parameters uncertainty, especially the vehicle mass and the cornering stiffness. Indeed, it is difficult to estimate accurately the stiffness of the tire since it is related to the road coefficient of friction, the type of the road, the vertical load, etc. Also, the vehicle mass could be poorly estimated or variable since it is dependent on the passengers and the amount of fuel. The controllers robustness was evaluated for different parameters values. We present in Fig. 20, using Scenario 1 (presented in Fig. 12), the lateral displacement error and the longitudinal speed regulated by the *I&I* based controller, the Lyapunov

based controller and the PD/PI controller for different values of the vehicle mass ($\pm 30\%$).

Fig. 21 shows the variation of the lateral error and the speed in the presence of cornering stiffness uncertainties ($\pm 30\%$) using the developed controllers and the PD/PI controller.

Regarding the longitudinal speed (Fig. 20b and Fig. 21b), we cannot extract important differences in the behavior of the controllers. In fact, only the transitory state of the speed regulation is affected by the mass uncertainties (Fig. 20b) but the three controllers present almost the same behavior. Moreover, the cornering stiffness uncertainties don't affect the longitudinal speed, regardless of the used controller (Fig. 21b).

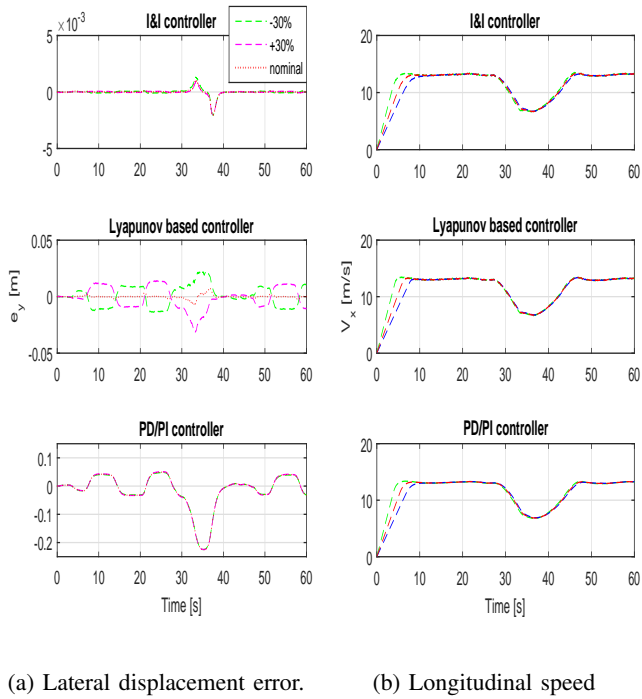


Fig. 20: Controllers robustness against uncertainties on the vehicle mass ($\pm 30\%$).

Regarding the lateral displacement error in Fig. 20a and Fig. 21a, some conclusions can be made: The lateral displacement error, produced when using the Lyapunov based control, increases with a non-null parameters uncertainty but remains acceptable even with a parameter uncertainty of $\pm 30\%$. The *I&I* controller is slightly affected by the parameters uncertainties. And the PD/PI controller is almost not affected by the parameters variations, because it does not depend on the parameters. However, it is clearly less performant than both other controllers.

In conclusion, both of the developed controllers and the classical PD/PI controller are able to follow the path and the desired speed with acceptable errors despite the parameters variations. However, the Lyapunov based controller is more sensitive to the parameters uncertainties than the *I&I* and the PD/PI controllers.

B. Controllers Experimental Validation

1) Presentation of the Experimental Environment:

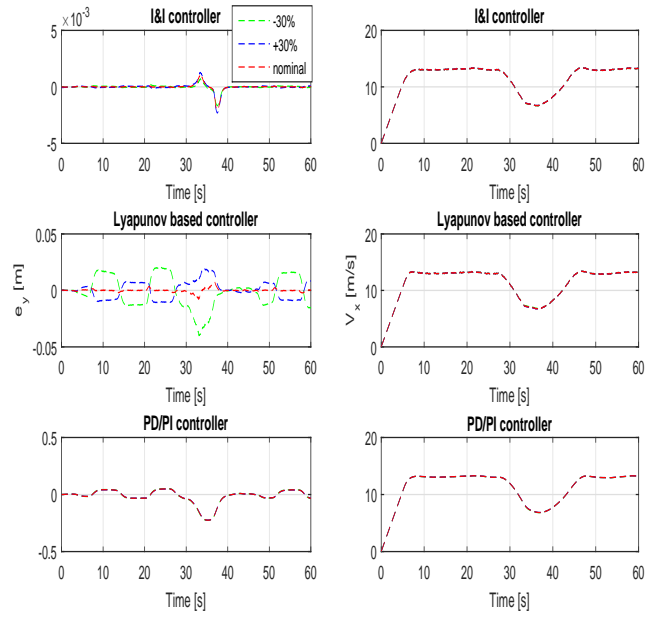


Fig. 21: Controllers robustness against uncertainties on the cornering stiffness ($\pm 30\%$).
(a) Lateral displacement error. (b) Longitudinal speed.

a) Automated vehicle description:

The experimental vehicle used to validate the controller is an autonomous vehicle (APACHE) based on ZOE cars from the equipment of the ROBOTEX project (see Fig. 22).

The APACHE car design presents several navigation modes [42]: A manual mode where the driver is in charge of the navigation, a cooperative mode that allows the driver to control at least one subsystem of the vehicle (acceleration/braking or steering) while the rest is done autonomously, and an autonomous navigation mode where the system manages both longitudinal and lateral controls of the vehicle. For safety reasons, any intervention from the driver in the autonomous mode automatically switches the vehicle to the manual mode. Moreover, the vehicle is limited to a maximum speed of 50 km/h while driving autonomously. The automated control of the vehicle is done through a dSpace MicroAutoBox prototyping hardware. It is designed to send controls such as the Driving/Braking motor torque and the steering wheel angle through the vehicle CAN bus. The autonomous vehicle is equipped with several sensors, meanwhile, to validate the developed controller, we make use of a Novatel's SPAN-CPT in order to have centimeter accuracy localization data. This system combines a Global Navigation Satellite System (GNSS) and an Inertial Navigation System (INS). In addition to Real Time Kinematic (RTK) corrections, the combined GNSS/INS solution can provide both absolute accuracy and continuity for localization. The SPAN is used with the higher frequency of the Inertial Measurement Unit (IMU), which corresponds to 50 Hz. The system provides information on localization (latitude, longitude, height), velocity (w.r.t. east, north, up directions), acceleration (lateral, longitudinal, vertical), rotation (roll, pitch, azimuth) and rotation rate (roll rate,

pitch rate, yaw rates). It also provides the standard deviations of the previously mentioned quantities.



Fig. 22: Experimental vehicle: ZOE.

b) Vehicle parameters:

To find the parameters of our vehicle ZOE, we have used the Scaner-Studio simulator. Many vehicles are modeled in this simulator which enables to create different driving scenarios, record necessary data, study the vehicles behavior and many other applications useful for an engineer or a researcher. From the given resources, a vehicle representing the vehicle ZOE is used. The extracted parameters given in the SI units are the following:

$$\begin{aligned} m &= 1456.4 \text{kg}, I_z = 2400 \text{kg.m}^2, m_{ij} = 15 \text{kg} \\ R_{eff} &= 0.30678 \text{m}, s = 2.22 \text{m}^2, I_w = 1.83 \text{kg.m}^2 \\ C_{\alpha_f} &= 77349 \text{N/rad}, C_{\alpha_r} = 77349 \text{N/rad} \\ L_f &= 1.0847 \text{m}, L_r = 1.5553 \text{m}, E = 1.546 \text{m}, c_d = 0.333. \end{aligned} \quad (59)$$

c) Sending Controls to the ZOE:

As mentioned above, the autonomous vehicle ZOE can be controlled via the Driving/Braking motor torque and the steering wheel angle. Contrariwise, our controller sends the Driving/Braking wheels torque and the steering angle that corresponds to the angle between the front tires and the vehicle longitudinal axis.

To do so, we estimated the relation between the motor torque (τ_m) and the torque transmitted to the wheels (τ_w) by measuring these two variables and comparing them. The established relation is as follows:

$$\tau_w = 9.3\tau_m - 46.5 \quad (60)$$

Remark: The low level architecture of the vehicle's driveline provides a non null wheels torque (of 46.5 N.m) when the motor torque is null. This torque, which we call ramping torque, aims to avoid a backward vehicle navigation when the motor torque is null, and the vehicle navigates on an inclined road segment. That's why, (60) shows that when the vehicle is stopped and the motor torque is null, the wheels torque is negative (-46.5N.m). In fact, this negative torque compensates the ramping torque and as result the wheels torque are also null when the vehicle is stopped.

Concerning the relation between the angle of the steering

wheel (δ_{sw}) and the real steering angle on the tires with respect to the vehicle direction (δ), we assume that there is a linear relation between these two angles. Referring to the documentation, a ratio of 14.04 exists between these two angles, so as:

$$\delta_{sw} = 14.04 \delta. \quad (61)$$

d) Experimental tracks: The track used to validate the controllers is called Seville and is located near the Heudiasyc laboratory. It consists of two J-turns related by a straight road segment (see Fig. 23). The track curvature is computed using a map of trajectory coordinates (X,Y) provided in the ENU frame.



Fig. 23: Experimental test track: Seville.

Fig. 24 shows the computed curvature of the test track Seville. The curvature reaches 0.13m^{-1} in the J-turn A and 0.1m^{-1} in the J-turn B. Then, when leaving the J-turn A, a curve having a curvature of almost 0.08m^{-1} must be tracked; note that the curvature varies rapidly on this road segment.

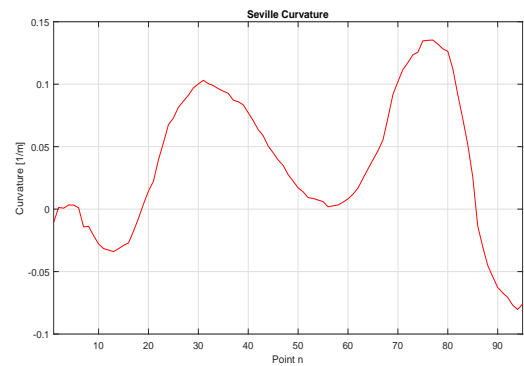


Fig. 24: Seville track curvature.

e) Control inputs tested experimentally: Many assumptions were made in order to simplify the task and to deal with the experimental limitations:

- In the Lyapunov based controller, the terms in \ddot{x} and $\ddot{\psi}$ in (37) were neglected based on the simulations analysis using the track Seville conditions and different speed profiles.
- Also in the Lyapunov based controller, the lateral speed in the vehicle frame (\dot{y}) and the vehicle yaw rate ($\dot{\psi}$) are estimated by their computed values at the equilibrium on

the desired trajectory given in (49), since their measured values were very noisy

In fact, when replacing \dot{y} and $\dot{\psi}$ by \dot{y}_{eq} and $\dot{\psi}_{eq}$, the equation (31) becomes:

$$\dot{s}_1 = -K_{lyy}s_1 + \frac{1}{m}[(F_{y_{fl}}^* + F_{y_{fr}}^* - F_{y_{rl}}^* - F_{y_{rr}}^*) - (F_{y_{fl}} + F_{y_{fr}} - F_{y_{rl}} - F_{y_{rr}})], \quad (62)$$

where $F_{y_{ij}}$ are the lateral forces and $F_{y_{ij}}^*$ are the equivalent of the lateral forces at the equilibrium point on the desired trajectory.

At this point, two hypotheses were made:

- The lateral stability is not lost, which means that $F_{y_{ij}}^* - F_{y_{ij}}$ is small.
- we assume that $F_{y_{ij}}^* - F_{y_{ij}}$ is bounded and converges to zero when the trajectory is reached.

By assuming that, the behavior of s_1 in a neighborhood of the equilibrium can be assimilated to:

$$\dot{s}_1 \simeq -K_{lyy}s_1, \quad (63)$$

and this guarantees the convergence of s_1 and by consequence the convergence of e_y and \dot{e}_y to zero.

- After many experiments on the track Seville, we found that the term in δ in the control input τ_w , computed by both of the coupled controllers, prevents the convergence of the longitudinal speed towards its desired value. In fact, the term in δ consists in an estimation of the sideslip angle. This estimation is very bad when the desired speed is not sufficiently high. Since the scenarios we executed on the experimental track were at low speed, we neglected the term in δ from the computation of the control law τ_w , knowing that its effect can be neglected.
- The integral term in τ_w was omitted in the tests executed for the moment.

As a result, the control inputs of the Lyapunov based controller used to control the experimental vehicle are as follows:

$$\begin{aligned} \tau_w = R_{eff}[m_e \ddot{x}^* - m_e(K_{lyx} + \lambda_x)e_{vx} - m\dot{y}_{eq}\dot{\psi}_{eq} \\ + L_3\dot{\psi}_{eq}^2 + F_{aero}] \end{aligned} \quad (64)$$

$$\begin{aligned} \delta = \frac{1}{2C_{\alpha_f}}[-mL_s\ddot{e}_\psi - m(K_{lyy} + \lambda_y)\dot{e}_{y_f} - mK_{lyy}\lambda_y e_{y_f} \\ + m\dot{x}^2\rho_{ref} + 2C_{\alpha_f} \frac{\dot{x}(\dot{y}_{eq} + L_f\dot{\psi}_{eq})}{\dot{x}^2 - (\frac{E}{2}\dot{\psi}_{eq})^2} + 2C_{\alpha_r} \frac{\dot{x}(\dot{y}_{eq} - L_r\dot{\psi}_{eq})}{\dot{x}^2 - (\frac{E}{2}\dot{\psi}_{eq})^2}], \end{aligned} \quad (65)$$

where the aerodynamic force is defined as in (6) by :

$$F_{aero} = 1/2 \rho_a c_d s \dot{x}^2,$$

where ρ_a is the mass density of air, s is the frontal area of the vehicle, c_d is the aerodynamic drag coefficient and \dot{x} is the longitudinal vehicle speed. s is taken from the ZOE model under Scaner-Sutio simulator.

The control inputs tested experimentally for the *I&I* controller are given by:

$$\begin{aligned} \tau_w = R_{eff}[m_e \ddot{x}^* - m_e(K_{imx} + \lambda_x)e_{vx} - m\dot{y}_{eq}\dot{\psi}_{eq} \\ + L_3\dot{\psi}_{eq}^2 + F_{aero}] \end{aligned} \quad (66)$$

$$\delta = u_1 + u_2 + \delta_{eqvl} \quad (67)$$

where u_1 , u_2 and δ_{eqvl} are given by (46) and (47).

The developed Lyapunov based controller and the *I&I* based controller were compared to a classical PD/P controller (the integral action was omitted in the PD/PI and in the coupled controllers as well). The control inputs of the PD/P controller are given in (57) and (58), where K_{ix} is set to zero.

2) Validation Results: The controllers were validated using many scenarios. We present in the following a test that was done on the track Seville with a desired speed of 15km/h. In this test, the gains of the controllers and the parameter L_s are set as follows:

$$\begin{aligned} K_{lyx} = 1, \quad K_{lyy} = 5, \quad \alpha_0 = 0.2, \quad \beta_0 = 0.0001 \\ K_{imx} = 1, \quad K_{dy} = 0.7, \quad K_{py} = 4, \quad K_{px} = 436 \\ \lambda_y = 3.5, \quad L_s = 3m. \end{aligned} \quad (68)$$

The speed tracking with the different controllers is shown in Fig. 25 while the Driving/Braking wheels torque generated by the different controllers are shown in Fig. 26. The Lyapunov and the *I&I* based controllers behave the same way since they are using the same control law for the longitudinal dynamics.

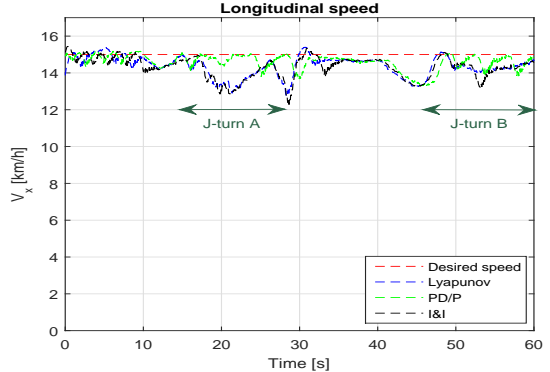


Fig. 25: Test on Seville, controllers comparison: Desired longitudinal speed tracking.

Fig. 27 shows the reference trajectory and the trajectory executed by the vehicle when using each of the three controllers. The lateral displacement errors at the COG are given in Fig. 28 and the steering angle on tires provided by each of the three controllers are shown in Fig. 29. We can observe that all the controllers succeed in tracking the reference trajectory with acceptable errors.

However, some differences can be noticed when leaving the J-turn A (see Fig. 27). Indeed, this part of the track is the most critical part since the road curvature changes fast and reaches high values for a few seconds (Fig. 24: point 75 to 91). When using the PD/P controller, the vehicle oscillates around the reference trajectory and the vehicle safety has been threatened (This test was repeated many times, and the driver was sometimes forced to decelerate in this driving zone). Contrariwise, the Lyapunov based controller and the *I&I* based one leave the J-turn A with almost the same

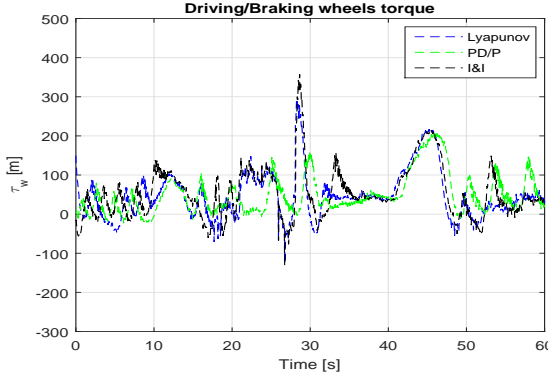


Fig. 26: Test on Seville, controllers comparison: Front wheels torque.

way (a smooth navigation) although the lateral error given by the Lyapunov based controller is smaller than that given by the *I&I* controller at this point. The behavior of the three controllers on the rest of the track Seville is almost the same. The oscillations caused by the PD/P controller when leaving the J-turn A could be explained by the delay presented in the controller reaction to the given driving situation. This delay was clearly felt during the experimental tests and can be seen in Fig. 29. For example, in this test, when leaving the J-turn A, at $t = 27.7\text{s}$ the coupled controllers are commanding a steering angle of about -35° while the PD/P controller is commanding a steering wheel angle of about -12° . This explains the oscillations of the vehicle trajectory provided by the PD/P controller. The reason for this delay is that both of the coupled controllers include an adaptive part in their control inputs and another part of the regulation while the PD/P controller includes only a regulation of the output. The presence of these adaptive parts of the coupled controllers allows the controller to anticipate the situation since they permit to approach to the desired value of the output, and the regulation is then done in a domain near the desired output value.

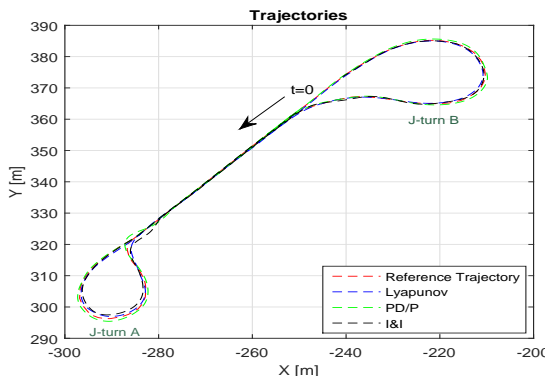


Fig. 27: Test on Seville, controllers comparison: Reference trajectory tracking.

Note that, even though the track Seville presents a critical driving zone (the road curvature changes fast and reaches high values for a few seconds at the exit of J-turn A), the test presented in this paper can't be considered an aggressive non-

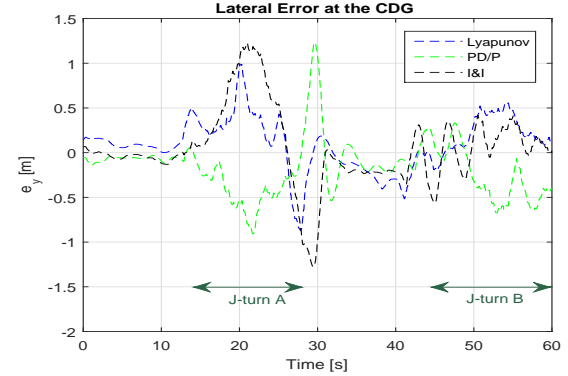


Fig. 28: Test on Seville, controllers comparison: Lateral displacement error.

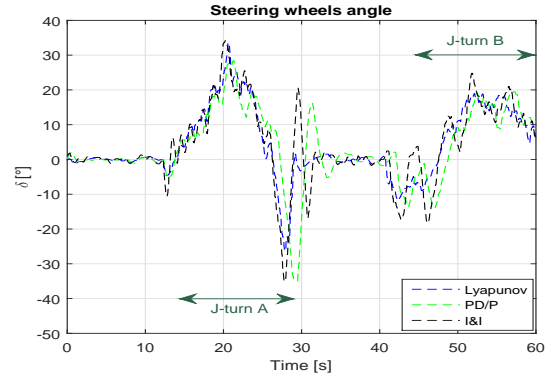


Fig. 29: Test on Seville, controllers comparison: Steering angle on front tires.

linear test. Indeed, the experimental test is executed at 15km/h , since the experimental track Seville does not allow to execute high speeds maneuvers. The lateral acceleration reaches its maximum at 2.59m/s^2 . This means that the executed test is not a highly non-linear driving scenario as in the simulation shown in Fig. 17, where the lateral acceleration reaches -7.5m/s^2 .

Based on the experimental tests conducted for the moment, and taking into account the assumptions that were made, we suggest that the optimal longitudinal tracking is performed by the linear PD/P controller while the optimal lateral tracking is performed by a nonlinear controller (in these conditions, both of the nonlinear controllers present very close performances).

V. CONCLUSION

This work deals with the autonomous vehicles navigation topic, mainly the trajectory tracking problem.

As a first step, a four wheeled planar vehicle model is developed using a multi-body formalism based on Euler-Lagrange algorithm. This model was then validated under Matlab/Simulink using data from the simulator Scaner-Studio. The validation showed good results validating thus the developed model in a wide margin of navigation. Based on this vehicle model, two coupled controllers are proposed. The first controller makes use of Lyapunov control technique while the second one is based on the Immersion

and Invariance with sliding mode approach. Beside ensuring a robust tracking of the reference trajectory and the desired speed profile, we aim to enhance the vehicle safety by taking into account the strong coupling between the lateral and the longitudinal vehicle dynamics, usually neglected when designing vehicle controllers.

The developed controllers are then validated by simulation under Matlab/Simulink and experimentally on a robotized vehicle ZOE in the Heudiasyc laboratory. The controllers behaviors were also compared between them and with a classical PD/PI controller. The preliminary results show a better performance of the coupled controllers compared to the PD/PI controller, especially in the critical driving conditions. However, the I&I controller shows to be more performant than the Lyapunov controller. This result can be explained by the fact that the Lyapunov based controller depends on the vehicle model much more than the I&I controller. And, since using a complete vehicle model to derive the control laws increases the problem complexity, the vehicle model used in this work was simplified by using some usual assumptions and a Linear model for the contact forces between the tires and the ground. This simplification affects the performance of the Lyapunov based controller and reduces its robustness. In order to ameliorates the controllers performances, we aim, as a perspective to this work, to use a more accurate tire model that takes into account the non-linearity of the Tire/Ground contact forces such as Dugoff's model, piece-wise linear model and others. Another important point that we believe can improve the controller's performances is the use of an adaptive formulation for the parameter L_s , that serves to compensate the lateral controllers/actuators delay, with respect to the vehicle speed and the reference trajectory curvature. In fact, the simulations have shown a very small sensibility towards the parameter L_s . However, the experimental tests have shown that the tuning of this parameter is not at all a simple task. When this parameter is over-tuned (its value is greater than necessary), the vehicle starts oscillating strongly; and when this parameter is under-tuned the reference trajectory tracking could fail. Also among the perspectives of this work, we look forward to study the impact of all the assumptions that had been made to simplify the controllers and to respond to the experimental limitations. In addition, the robustness of the coupled controllers should be compared experimentally with more scenarios, with higher speeds and stronger non-linearity conditions in order to be able to conclude about the controllers robustness at the limits of stability of the vehicle.

ACKNOWLEDGMENT

This work was carried out in the framework of the Labex MS2T, which was funded by the French Government, through the program Investments for the future managed by the National Agency for Research (Reference ANR-11-IDEX-0004-02) and the framework of the Equipex ROBOTEX (Reference

ANR-10-EQPX-44-01), which was funded by the French Government, through the program Investments for the future managed by the National Agency for Research.

REFERENCES

- [1] R. Marino, S. Scalzi, and M. Netto, "Nested pid steering control for lane keeping in autonomous vehicles," *Control Engineering Practice*, vol. 19, no. 12, pp. 1459–1467, 2011.
- [2] A. Benine-Neto and S. Mammar, "Piecewise affine state feedback controller for lane departure avoidance," *IEEE Intelligent Vehicles Symposium (IV)*, pp. 839–844, 2011.
- [3] J. Pérez, J. Godoy, V. Milanés, J. Villagrá, and E. Onieva, "Path following with backtracking based on fuzzy controllers for forward and reverse driving," *IEEE Intelligent Vehicles Symposium (IV)*, pp. 1108–1113, 2012.
- [4] L. Nehoua and L. Nouvelière, "Backstepping based approach for the combined longitudinal-lateral vehicle control," *IEEE Intelligent Vehicles Symposium (IV)*, pp. 395–400, 2012.
- [5] G. Tagne, R. Talj, and A. Charara, "Higher-order sliding mode control for lateral dynamics of autonomous vehicles, with experimental validation," *IEEE Intelligent Vehicles Symposium (IV)*, pp. 678–683, 2013.
- [6] S. Hima, B. Lussetti, B. Vanholme, S. Glaser, and S. Mammar, "Trajectory tracking for highly automated passenger vehicles," *18th World Congress IFAC*, vol. 44, no. 1, pp. 12 958–12 963, 2011.
- [7] Y. Abbassi, Y. Ait-Amirat, and R. Outbib, "Nonlinear feedback control of vehicle speed," *18th World Congress IFAC*, vol. 44, no. 1, pp. 6279–6284, 2011.
- [8] J. Naranjo, C. González, J. Reviejo, R. García, and T. D. Pedro, "Adaptive fuzzy control for inter-vehicle gap keeping," *IEEE Transactions on Intelligent Transportation Systems*, vol. 4, no. 3, pp. 132–142, 2003.
- [9] A. Ferrara and C. Vecchio, "Second order sliding mode control of vehicles with distributed collision avoidance capabilities," *Mechatronics*, vol. 19, no. 4, pp. 471–477, 2009.
- [10] L. Nouveliere *et al.*, "Experimental vehicle longitudinal control using a second order sliding mode technique," *Control Engineering Practice*, vol. 15, no. 8, pp. 943–954, 2007.
- [11] M. Eilers and C. Möbus, "Learning the human longitudinal control behavior with a modular hierarchical bayesian mixture-of-behaviors model," *IEEE Intelligent Vehicles Symposium (IV)*, pp. 540–545, 2011.
- [12] B. D'Andréa-Novel, C. Boussard, M. Fliess, O. E. Hamzaoui, H. Mounier, and B. Steux, "Commande sans modèle de la vitesse longitudinale d'un véhicule électrique," in *Sixième Conférence Internationale Francophone d'Automatique (CIFA 2010)*, Nancy, France, 2010.
- [13] E. Lim, "Lateral and longitudinal vehicle control coupling in the automated highway system," Ph.D. dissertation, University of California at Berkeley, 1998.
- [14] L. Menhour, B. D'Andréa-Novel, M. Fliess, and H. Mounier, "Coupled nonlinear vehicle control: Flatness-based setting with algebraic estimation techniques," *Control Engineering Practice*, vol. 22, pp. 135–146, 2014.
- [15] R. Attia, R. Orjuela, and M. Basset, "Combined longitudinal and lateral control for automated vehicle guidance," *Vehicle Systems Dynamics*, vol. 52, no. 2, pp. 261–279, 2014.
- [16] R. Rajamani, *Vehicle dynamics and control*. Springer Science & Business Media, 2011.
- [17] S. Thrun, M. Montemerlo, H. Dahlkamp, D. Stavens, A. Aron, J. Diebel, P. Fong, J. Gale, M. Halpenny, G. Hoffmann *et al.*, "Stanley: The robot that won the darpa grand challenge," *Journal of field Robotics*, vol. 23, no. 9, pp. 661–692, 2006.
- [18] G. Baffet, "Développement et validation expérimentale d'observateurs des forces du contact pneumatique/chaussée d'une automobile," Ph.D. dissertation, Université de Technologie de Compiègne, 2007.
- [19] U. Kiencke and L. Nielsen, *Automotive control systems*. Springer, 2005, vol. 2.
- [20] R. Sharp, "The stability and control of motorcycles," *Journal of mechanical engineering science*, vol. 13, no. 5, pp. 316–329, 1971.
- [21] V. Cossalter and R. Lot, "A motorcycle multi-body model for real time simulations based on the natural coordinates approach," *Vehicle system dynamics*, vol. 37, no. 6, pp. 423–447, 2002.
- [22] E. Sanjurjo, "State observers based on detailed multibody models applied to an automobile," Ph.D. dissertation, University of A Coruna, 2016.

- [23] J. Cuadrado, D. Dopico, M. Naya, and M. González, "Penalty, semi-recursive and hybrid methods for mbs real-time dynamics in the context of structural integrators," *Multibody System Dynamics*, vol. 12, no. 2, pp. 117–132, 2004.
- [24] D. Dopico, F. González, J. Cuadrado, and J. Kőveses, "Determination of holonomic and nonholonomic constraint reactions in an index-3 augmented lagrangian formulation with velocity and acceleration projections," *Journal of Computational and Nonlinear Dynamics*, vol. 9, no. 4, p. 041006, 2014.
- [25] S. Maakaroun, "Modélisation et simulation dynamique d'un véhicule urbain innovant en utilisant le formalisme de la robotique," Ph.D. dissertation, Université Nantes Angers Le Mans, 2011.
- [26] S. Maakaroun, P. Chevrel, M. Gautier, and W. Khalil, "Modelling and simulation of a two wheeled vehicle with suspensions by using robotic formalism," *18th World Congress IFAC*, vol. 44, no. 1, pp. 2156–2161, 2011.
- [27] G. Venture, "Identification des paramètres dynamiques d'une voiture," Ph.D. dissertation, Ecole Centrale de Nantes, Université de Nantes, 2003.
- [28] G. Max and B. Lantos, "Modeling and control of tree-like structured vehicles and robots using appell method," *IEEE 13th International Symposium on Intelligent Systems and Informatics (SISY)*, pp. 223–228, 2015.
- [29] J. Luh, M. Walker, and R. Paul, "On-line computational scheme for mechanical manipulators," *J. DYN. SYS. MEAS. and CONTR.*, vol. 102, pp. 69–76, 1980.
- [30] W. Khalil and E. Dombre, *Modeling, identification and control of robots*. Butterworth-Heinemann, 2004.
- [31] N. Ding and S. Taheri, "A modified dugoff tire model for combined-slip forces," *Tire Science and Technology*, vol. 38, no. 3, pp. 228–244, 2010.
- [32] Oktal, *Driving simulation engine scaner*. <http://www.scanersimulation.com>, 2016.
- [33] A. Chebly, R. Talj, and A. Charara, "Coupled longitudinal and lateral control for an autonomous vehicle dynamics modeled using a robotics formalism," *20th World Congress IFAC*, vol. 50, no. 1, pp. 12 526–12 532, 2017.
- [34] H. Dugoff, P. Fancher, and L. Segel, "An analysis of tire traction properties and their influence on vehicle dynamic performance," SAE Technical Paper, Tech. Rep., 1970.
- [35] A. Astolfi, D. Karagiannis, and R. Ortega, *Nonlinear and adaptive control with applications*. Springer Science & Business Media, 2007.
- [36] Y. Shtessel, C. Edwards, L. Fridman, and A. Levant, *Sliding mode control and observation*. Springer, 2014.
- [37] V. I. Utkin, *Sliding modes in control and optimization*. Springer Science & Business Media, 2013.
- [38] A. Levant, "Robust exact differentiation via sliding mode technique," *automatica*, vol. 34, no. 3, pp. 379–384, 1998.
- [39] A. Levant, "Chattering analysis," *IEEE transactions on automatic control*, vol. 55, no. 6, pp. 1380–1389, 2010.
- [40] A. Chebly, G. Tagne, R. Talj, and A. Charara, "Local trajectory planning and tracking of autonomous vehicles, using clothoid tentacles method," in *Intelligent Vehicles Symposium (IV)*. IEEE, 2015, pp. 674–679.
- [41] A. Chebly, R. Talj, and A. Charara, "Maneuver planning for autonomous vehicles, with clothoid tentacles for local trajectory planning," in *Intelligent Transportation Systems (ITSC)*. IEEE, 2017, pp. 1–6.
- [42] P. Xu, G. Dherbomez, E. Hry, A. Abidli, and P. Bonnifait, "System architecture of a driverless electric car in the grand cooperative driving challenge," *IEEE Intelligent Transportation Systems Magazine (ITS Mag.)*, vol. 10, no. 1, pp. 47–59, 2018.